Naval Research Laboratory

Washington, DC 20375-5000

Bathymetric Hazard Survey Test (BHST Report No. 3), Scientific Results and FY 1982-1984 Processing

F. T. ERSKINE, G. M. BERNSTEIN, S. M. BRYLOW, W. T. NEWBOLD,
R. C. GAUSS, E. R. FRANCHI, AND B. B. ADAMS

Large Aperture Acoustics Branch
Acoustics Division

August 20, 1987

REPORT DOCUMENTATION PAGE

1a. REPORT SECURITY CLASSIFICATION UNCLASSIFIED	1b. RESTRICTIVE MARKINGS
2a. SECURITY CLASSIFICATION AUTHORITY	3. DISTRIBUTION/AVAILABILITY OF REPORT
2b. DECLASSIFICATION/DOWNGRADING SCHEDULE	Approved for public release; distribution unlimited.

4. PERFORMING ORGANIZATION REPORT NUMBER(S) NRL Report 9048	5. MONITORING ORGANIZATION REPORT NUMBER(S)

6a. NAME OF PERFORMING ORGANIZATION Naval Research Laboratory	6b. OFFICE SYMBOL (If applicable) Code 5160	7a. NAME OF MONITORING ORGANIZATION

6c. ADDRESS (City, State, and ZIP Code) Washington, DC 20375-5000	7b. ADDRESS (City, State, and ZIP Code)

8a. NAME OF FUNDING/SPONSORING ORGANIZATION (See page ii)	8b. OFFICE SYMBOL (If applicable) Code 500	9. PROCUREMENT INSTRUMENT IDENTIFICATION NUMBER

8c. ADDRESS (City, State, and ZIP Code) NSTL Station, MS 39529	10. SOURCE OF FUNDING NUMBERS

PROGRAM ELEMENT NO.	PROJECT NO.	TASK NO.	WORK UNIT ACCESSION NO.
62435N	RJ35Q14-000		DN180-351

11. TITLE (Include Security Classification)

Bathymetric Hazard Survey Test (BHST Report No. 3), Scientific Results and FY 1982-1984 Processing

12. PERSONAL AUTHOR(S)
Erskine, F. T., Bernstein, G. M., Brylow, S. M., Newbold, W. T., Gauss, R. C., Franchi, E.R. and Adams, B. B.

13a. TYPE OF REPORT Final	13b. TIME COVERED FROM 10/1/82 TO 9/30/84	14. DATE OF REPORT (Year, Month, Day) 1987 August 20	15. PAGE COUNT 54

16. SUPPLEMENTARY NOTATION

17. COSATI CODES			18. SUBJECT TERMS (Continue on reverse if necessary and identify by block number)
FIELD	GROUP	SUB-GROUP	Reverberation Seamount heights Ocean topography
			Acoustic backscatter Acoustic mapping Bathymetry (Continues)

19. ABSTRACT (Continue on reverse if necessary and identify by block number)

The Naval Research Laboratory is developing a long range active acoustics technique for estimating seamount heights and mapping undersea topography over an entire ocean basin region. A concept demonstration, the Bathymetric Hazard Survey Test (BHST) was conducted in the eastern Atlantic in 1980. The technique uses explosive shot acoustic sources and a large aperture, towed acoustic receiver array. Reverberation data are output to an imaging system to study the spatial distribution of acoustic backscatter. These images are in the form of two-dimensional maps of reverberation, each typically 2000 km on a side. After correction of maps from individual shot detonations for range-dependent propagation loss, and scattering area, we average maps together on a pixel by pixel basis for a clear picture of major bathymetry. We use measured backscattering strengths to estimate seamount heights for all major seamounts in a deep (5 km) basin to within ±1.3 km. This result is comparable to, or better than, that available from other wide area bathymetry surveying methods (e.g. aeromagnetics, gravimetry, and spacecraft altimetry). We can detect and locate all

(Continues)

20. DISTRIBUTION/AVAILABILITY OF ABSTRACT ☒ UNCLASSIFIED/UNLIMITED ☐ SAME AS RPT. ☐ DTIC USERS	21. ABSTRACT SECURITY CLASSIFICATION UNCLASSIFIED
22a. NAME OF RESPONSIBLE INDIVIDUAL Fred T. Erskine	22b. TELEPHONE (Include Area Code) (202) 767-3149 22c. OFFICE SYMBOL Code 5160

DD FORM 1473, 84 MAR   83 APR edition may be used until exhausted.   SECURITY CLASSIFICATION OF THIS PAGE
All other editions are obsolete

8a. NAME OF FUNDING/SPONSORING ORGANIZATION

Defense Mapping Agency/Naval Ocean Research and Development Activity

18. SUBJECT TERMS (Continued)

Image processing	Ray tracing	Ambient noise
Scattering strength	Beamforming	Sidelobe suppression
Long range sonar	Wide field sonar	Propagation loss
Transmission loss	Ocean basin survey techniques	BHST

19. ABSTRACT (Continued)

"major" (within about 2 km of the surface) seamounts in a deep basin to within ±20 km and can identify smaller ones as well. This is the last of three reports on BHST. We describe in detail our analysis of BHST data during the period FY 1982-84, with emphasis on seamount height estimation, topography mapping, and confidence estimates for our results.

CONTENTS

EXECUTIVE SUMMARY

This is the third in a series of three reports on the Bathymetric Hazard Survey Test (BHST), a proof-of-concept reverberation mapping experiment that was conducted in the eastern Atlantic Ocean in 1980. The purpose of BHST is to demonstrate that it is possible to map an entire ocean basin region approximately 2000 × 2000 km for the presence of major bathymetry (e.g., seamounts and ridges), with only about one week of sea test time, and to demonstrate the feasibility of this technique for determination of seamount heights. Our experimental method is straightforward. An explosive sound source is detonated near the center of an ocean basin and we measure the round trip travel time from source to reflectors and return. We assume that distance to backscattering topography is proportional to half the round trip time, with a proportionality constant equal to the sound speed. A multielement receiving array is used to determine the azimuthal directions to topographic features. Reverberation data are output to an imaging system to study the spatial distribution of acoustic backscatter. The images are in the form of two-dimensional maps of reverberation. Typical maps are larger than 2000 × 2000 km (or area greater than 4×10^6 km^2). After correction of maps from individual shot detonations for range-dependent propagation loss, we average maps together on a pixel by pixel basis for a clear picture of major bathymetry.

The two earlier reports in the series, BHST Report #1 [Franchi and Schifter, 1980], and BHST Report #2 [Schifter and Franchi, 1981] described the details of the experiment and preliminary results based on quick-look-at-sea data processing. The emphasis of this report is on the results from a more complete analysis of the BHST data at the Naval Research Laboratory during the fiscal years (FY) 1982-84. We discuss our analysis of ocean bottom reverberation data to estimate seamount heights and map all major undersea topography in the Canary Basin, and give confidence estimates for our results. After presenting the results, we discuss in more detail the data processing and analysis procedures that we developed and used to get those results. In Appendix A we discuss confidence limits for our seamount height regression analysis. Finally, for those who may be interested in our software, we present a more detailed description of our FORTRAN analysis programs for reverberation mapping in Appendix B.

In brief, our major new results from this analysis are:

A. We are able to estimate seamount heights for all major seamounts in a deep basin (typically 5 km depth) to within ±1.3 km.

B. We can detect and locate all "major" (within about 2 km of the surface) seamounts in a deep basin to within ±20 km and can identify many smaller seamounts as well (to depths as great as about 5 km).

C. We can accomplish (A) and (B) with about a week of sea test time.

D. We can display (A) and (B) as a two-dimensional bathymetry map.

REFERENCES

E.R. Franchi and D.E. Schifter, "Bathymetric Hazard Survey Test: Test Results," BHST Report No. 1, Acoustic Division, Naval Research Laboratory, Washington, DC, 1980.

D.E. Schifter and E.R. Franchi, "Bathymetric Hazard Survey Test: FY81 Processing," BHST Report No. 2, Acoustics Division, Naval Research Laboratory, Washington, DC, 1981.

BATHYMETRIC HAZARD SURVEY TEST (BHST REPORT NO. 3) SCIENTIFIC RESULTS AND FY 1982-1984 PROCESSING

1.0 INTRODUCTION

The Bathymetric Hazard Survey Test (BHST) was a proof-of-concept experiment conducted by the Naval Research Laboratory (NRL) in the eastern Atlantic Ocean in September 1980 [Franchi and Schifter, 1980; Schifter and Franchi, 1981].

The purpose of BHST is to demonstrate that it is possible to map an entire ocean basin region approximately 2000 × 2000 km for the presence of major bathymetry (e.g., seamounts and ridges) with only about 1 week of sea test time and to demonstrate the feasibility of this technique for determination of seamount heights. The test concept uses vertical line arrays of explosive charges as acoustic sources, and a horizontally deployed, linear array of hydrophones as a receiver, with a single ship towing platform. The technique uses backscattered acoustic energy from undersea geographic features. Received data are recorded on a high-density digital recorder (HDDR). These tapes are processed at NRL to convert the received acoustic signatures into two-dimensional maps of backscattered intensity that are then related to bathymetry location and size. The processing techniques are suitable for implementation in an on-board system in future applications.

Our results show that this active acoustic technique provides a relatively inexpensive method for a rapid survey of an entire ocean basin for the presence of major bathymetric features and is well suited for quick-look surveys of ocean basin areas that at present have been mapped only to a limited extent. We demonstrate that with this technique it is possible to measure the heights of all major topographic features in a basin to within ±1.3 km. The BHST technique provides a powerful ocean mapping tool for uncharted areas that will highlight locations suitable for high resolution, but narrow coverage mapping by other methods such as side scan sonar (e.g., Hussong et al., 1983).

The low-frequency reverberation mapping method that we describe in this report complements other techniques currently under development for large-scale ocean bathymetry mapping, i.e., spacecraft altimetry [Marsh et al., 1980; Haxby et al., 1983] and airborne magnetics/gravimetrics [Feden et al., 1979; Brozena, 1984].

BHST Report #1 [Franchi and Schifter, 1980] gives details of the sea test, while BHST Report #2 [Schifter and Franchi, 1981] discusses mapping efforts that used a hardware-based time domain beamformer while the ship was in transit after the close of the sea test. In this report we describe in detail our full-scale laboratory processing of the recorded data that was done in two phases: the first in fiscal year (FY) 1982 and the last in FY 1984. During these years, nominal funding was available to develop software to convert the raw data into acoustic maps. During FY 1983 this project was unfunded, although we continued a low-level processing effort on internal funds. Preliminary reverberation mapping results from our laboratory processing of BHST data are presented in conference proceedings [Erskine et al., 1983; Erskine and Franchi, 1984; and Erskine et al., 1985].

BHST is a logical follow-up to two earlier experiments performed by NRL in 1976 and 1979 called TOPO I and TOPO II respectively [Schifter et al., 1979 and 1986]. These earlier experiments

were conducted in a deep basin approximately 1000 km northeast of New Zealand. The TOPO experiments used omnidirectional explosive sources and a relatively low-resolution towed receiver array, but they showed that this acoustic mapping technique works and led to the BHST.

Historically, the TOPO and BHST experiments were preceded by early topographic ranging tests with very limited receiver directionality and ranging capability [Luskin et al., 1952; Halley, 1957; Whitmarsh, 1971; Spindel and Heirtzler, 1972]. In addition, applications of low-frequency topographic reverberation in an Arctic environment are discussed by the following: Zittel, 1979; Williams, 1981; Dyer et al., 1982 and 1983; Grantz and Hart, 1984; Dyer, 1984.

2.0 SCIENTIFIC RESULTS FROM BHST

In sections 2.1 through 2.3 we present the scientific results from the analysis of BHST ocean bottom reverberation data. For readers who wish to have additional details, we defer the bulk of the discussion of our reverberation computer processing and analysis steps to Section 3.

2.1 Estimation of Seamount Heights from Reverberation Data

The highest priority objective in our analysis of reverberation data from BHST is to develop a remote sensing method for estimating the heights of all major topographic relief in a deep ocean basin. Figure 1 is a schematic illustration of our experimental geometry. We deployed explosive sound sources at 4-h intervals and digitally recorded the topographic backscattered signals by using a directional receiver array. These signals are processed to yield received levels as a function of time and azimuth (we call these "beam-time" data files). By assuming a mean sound speed to relate arrival time to range, and by using information about receiver orientation and shot location, we are able to transform from time-azimuth format to latitude-longitude format to make a "single-shot" backscatter (reverberation) map for each shot detonation. We now describe the results of our analysis for seamount heights, based on these single-shot reverberation maps.
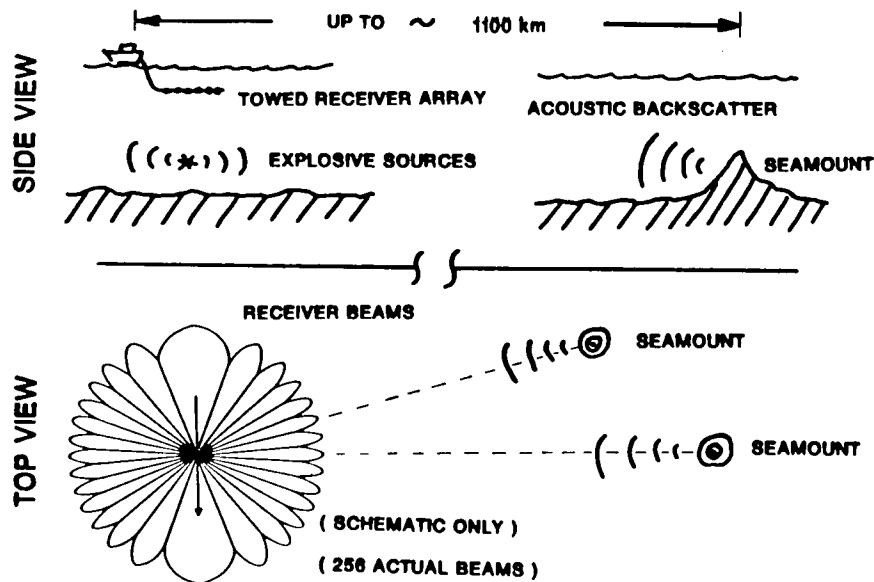

Fig. 1 — Geometry of the seamount height experiment

We have developed a set of analysis procedures for estimating the heights of seamounts and other major ocean topography from our reverberation data. The details of these analysis steps are presented in Section 3.3. In essence, we base this analysis on our two-dimensional, single-shot reverberation level maps (Section 3.2). We search along selected great cricle radials from the position of a shot detonation, through the positions of undersea topographic features, as guided by an existing bathymetry map of the Canary Basin area. We use the range-dependent NRL Reverberation Ray Trace Model [Franchi et al., 1984] to make estimates of propagation losses along these radials. We calculate estimates of equivalent "flat-bottom" backscattering area and use our known source level to compute a measure, SS, related to a range-independent back-scattering strength.

We then correlate this backscattering strength measure with seamount heights and slopes from archival bathymetry. Figure 2 shows the results of our correlation analysis for approximately 32 topographic features along 22 separate radials from 12 different shot detonations. The topography upon which Fig. 2 is based varied from small features only 800 to 1000 m above the nominal 5500 m basin depth to islands reaching the surface. These topographic features were at a variety of ranges from the source and receiver, from about 200 km at the nearest to about 1100 km at the farthest. Figure 2 shows that it is possible to remotely measure the heights of seamounts in an ocean basin by long range acoustic backscatter. The scattering strength measure SS is linearly correlated with bathymetry height relative to a nominal 5.5 km basin depth.

Figure 2 indicates that SS increases approximately 7 dB per km of seamount height. Since we have computed SS by use of a simple flat bottom scattering area assumption, this increase of SS with height may be due in part to the contribution of the actual seamount cross-sectional scattering area. We do not know if this 7 dB/km holds only for seamounts in the Canary Basin or if it is a more general descriptor of seamount backscatter.
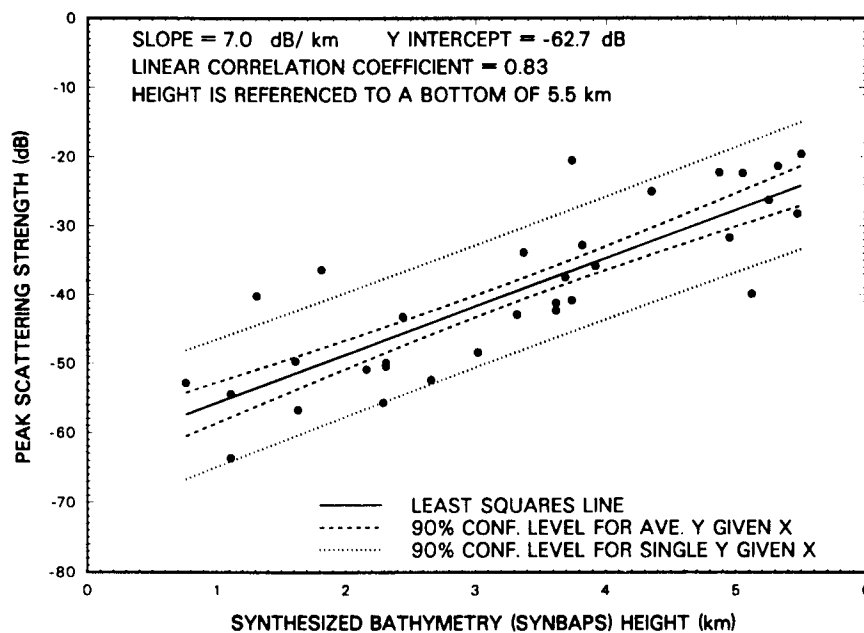

Fig. 2 — Peak "scattering strength measure" vs SYNBAPS bathymetry height
(re 5500 m depth)

Figure 3 shows an alternate way to present the data of Fig. 2. Here we have taken the linear least squares fitting function from Fig. 2 as our standard and asked the question: what is the reverberation-predicted bathymetry height for each data point in Fig. 2? We achieve this by a simple linear transformation, resulting in Fig. 3, a plot of predicted bathymetry height vs archival bathymetry height. The least squares fits of Figs. 2 and 3 have correlation coefficients of about 0.8. The 90% confidence curves (Appendix A) associated with these fits imply that we can predict bathymetry heights from long range reverberation to within about ±1.3 km.
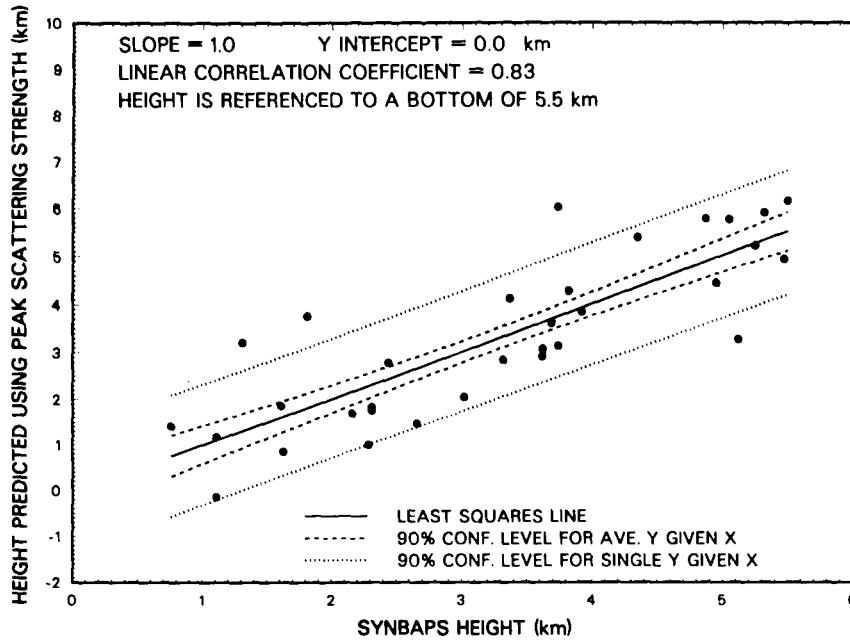

Fig. 3 — Reverberation predicted bathymetry heights vs SYNBAPS bathymetry height
(re 5500 m depth)

In similar fashion, we correlate SS with mean seamounts slopes from archival bathymetry. The results of this correlation are shown in Figs. 4 and 5. These plots show that SS is linearly correlated with seamount slopes as well as heights. The linear correlation coefficient for Figs. 4 and 5 is about 0.5, and the implied uncertainty in prediction of slopes from long range reverberation is about ±3° (90% confidence; see Appendix A). The correlation coefficient of 0.5 indicates that SS is only weakly correlated with seamount slopes. We have examined the correlation of seamount slope vs seamount height for our population of seamounts and find that the least squares fit has a correlation coefficient of 0.7 (90% confidence level) with slope of 0.7 deg/km. Thus, for this population of seamounts the higher seamounts appear to have greater slopes.

We are also interested in our ability to predict seamount position or range along a given radial from the reverberation time history. The acoustic backscatter will in general originate from the facing slopes of seamounts or bathymetric features, and thus we expect a position offset between the reverberation signatures and the centroids of seamounts. Figure 6 shows the range of reverberation SS peaks vs range of seamount peaks (centroids) for our sample radials. Figure 6 shows that we are able to predict seamount positions quite well but with a slight systematic offset (generally less than 15 km). We can readily correct for this radial offset to obtain actual seamount positions.
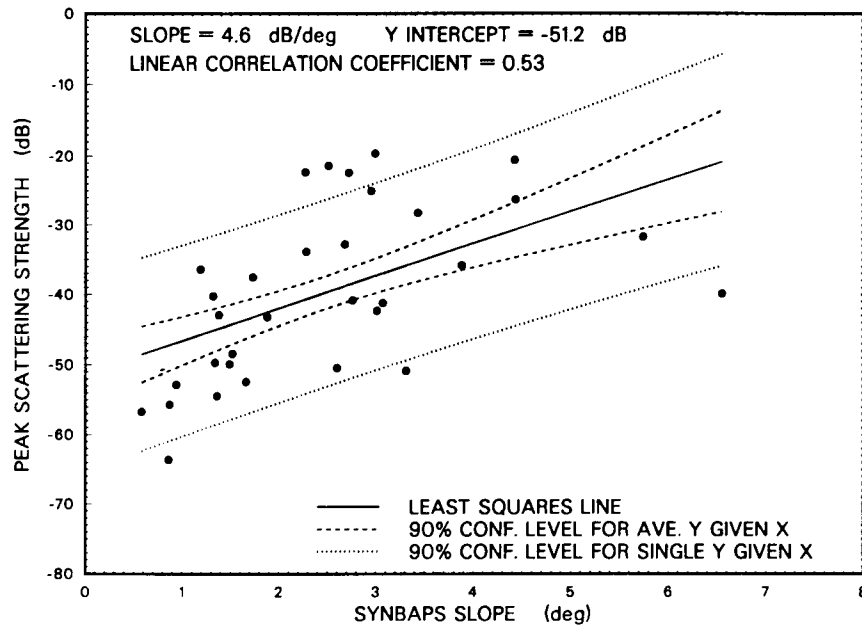
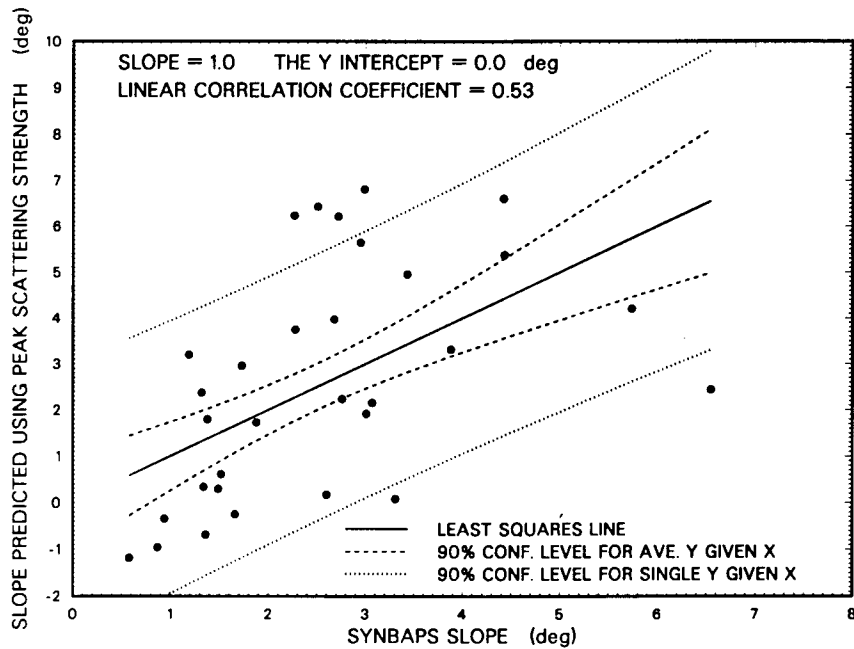Fig. 4 — Peak scattering strength measure vs SYNBAPS bathymetry slope

Fig. 5 — Reverberation predicted bathymetry slope vs SYNBAPS bathymetry slope
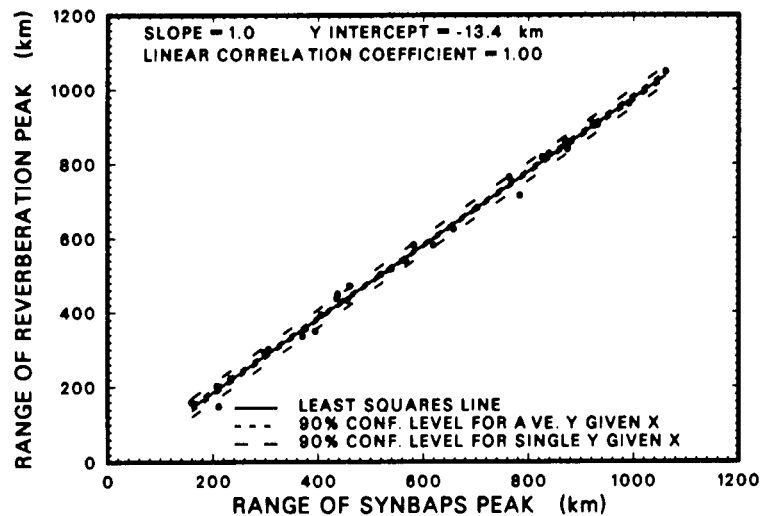
5

Fig. 6 — Range of reverberation peak vs range of SYNBAPS bathymetry

Since we can remotely estimate seamount positions, heights, and slopes we can illustrate estimated bathymetry along a selected radial and compare it to archival bathymetry [Van Wyckhouse, 1973]. Figure 7 presents such a bathymetry "estimation" for a typical radial and represents our initial effort to remotely estimate bathymetry in a deep ocean basin from long range reverberation returns. The method outlined above could be used in a less well-charted ocean basin than the one that we have studied (the Canary Basin). We would again derive functional relationships between scattering strength measure SS and seamount heights, slopes, and radial ranges by using a population of known seamounts. We would then apply these measured functions to estimate heights, slopes, and positions of uncharted seamounts.
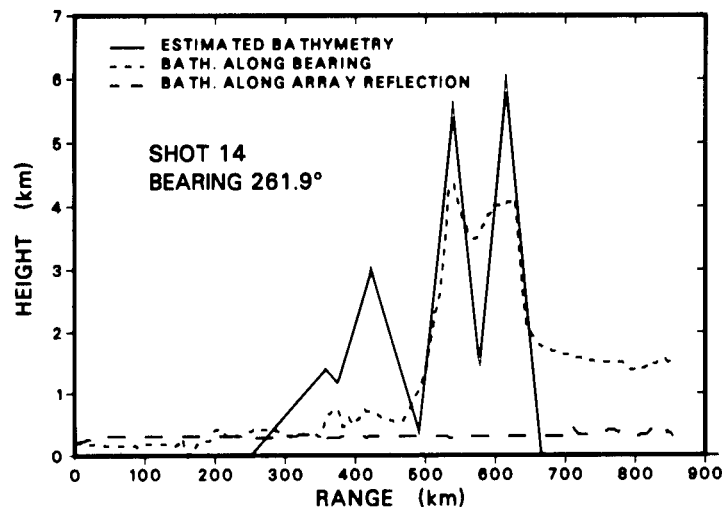

Fig. 7 — Reverberation estimated bathymetry compared to
SYNBAPS bathymetry for typical radial

We may compare our bathymetry height estimations to those from remote sensing techniques currently under development for wide area estimates of bathymetry. Each of these techniques depends critically on a physical model relating the physical quantity measured to topographic size. These techniques and the physical quantity measured in each case include spacecraft altimetry, which measures sea surface height relative to a nominal mean [Dixon et al., 1983], aeromagnetics, which measures the deviation of Earth's magnetic flux density from local mean [Feden et al., 1979; Czarnecki 1984], and airborne gravimetry, which measures the deviation of earth's gravitational acceleration from local mean [Brozena, 1984a, 1984b]. In each case, the relationship between the measured quantity and the actual bathymetry height is not uniquely given by a physical or mathematical model. At present the typical uncertainties in estimation of seamount heights by these techniques, when applied to a deep ocean basin under optimal conditions are approximately ±500 m to several kilometers, ±500 m to several kilometers; and hundreds of meters to several kilometers depending on type of basement, respectively. Thus, our seamount height estimation technique using long range reverberation compares favorably against these other techniques. Further refinements in the analysis procedures may reduce the uncertainty and merit investigation.

2.2 Mapping of Ocean Topography from Reverberation Data

The second major scientific objective in our analysis of BHST ocean bottom reverberation data is to develop a remote sensing technique for locating all "major" undersea topography (i.e., depth within several kilometers of the sea surface) in a deep basin. We now discuss the results of our reverberation mapping analysis.

We have referred to our use of reverberation maps to extract information about seamount heights in Section 2.1. The details of the digital processing and analysis related to our single-shot reverberation maps are presented in Sections 3.1 and 3.2. In brief, we deploy explosive sound sources at 4-h intervals and digitally record the backscattered signals from topography on a directional receiver array. These signals are processed to yield received levels as a function of time and azimuth. We assume that range to a seamount or other topographic feature is equal to the product of the mean sound speed multiplied by half the round trip travel time for scattered sound energy. By using information about receiver orientation and shot location, we are able to transform from time-azimuth format to latitude-longitude format, to make a "single-shot" map for each shot detonation. It is these maps (see Section 3.2) that we have used in our seamount height study (Sections 2.1 and 3.3).

We have developed an analysis method to average such digital single-shot map images together to make a fairly clear picture of major bathymetry in the Canary Basin. The details of this map "integration" method are presented in Section 3.4. In this section we present the end result of such a reverberation map averaging procedure, as applied to our BHST data. Figure 8 shows an integrated reverberation bathymetry map based on averaging 10 single-shot maps together. This map is 21° 20' × 21° 20' (almost 2000 km on a side). The gray level scale represents reverberation-estimated bathymetry height.

We have compared Figure 8 to archival bathymetry maps for the Canary Basin in order to identify the major topography corresponding to the bright patches on Fig. 8. We have associated the reverberation signatures (as seen on Fig. 8) with archival bathymetry by letters A through R (clockwise) on this figure: A through C are backscatter from a seamount chain containing over a dozen major seamounts, including Great Meteor Seamount (A) and Cruiser Seamount (B); D is from a rise associated with the East Azores Fracture Zone; E and F are from seamounts; G through I are from another seamount chain; J is from the Madeira Islands; K is from a seamount group; L is from a seamount; M through N are from the Canary Islands; O through Q are from a seamount group including Echo Seamount (O), Papp Seamount (P), and Tropic Seamount (Q); R is from a seamount.
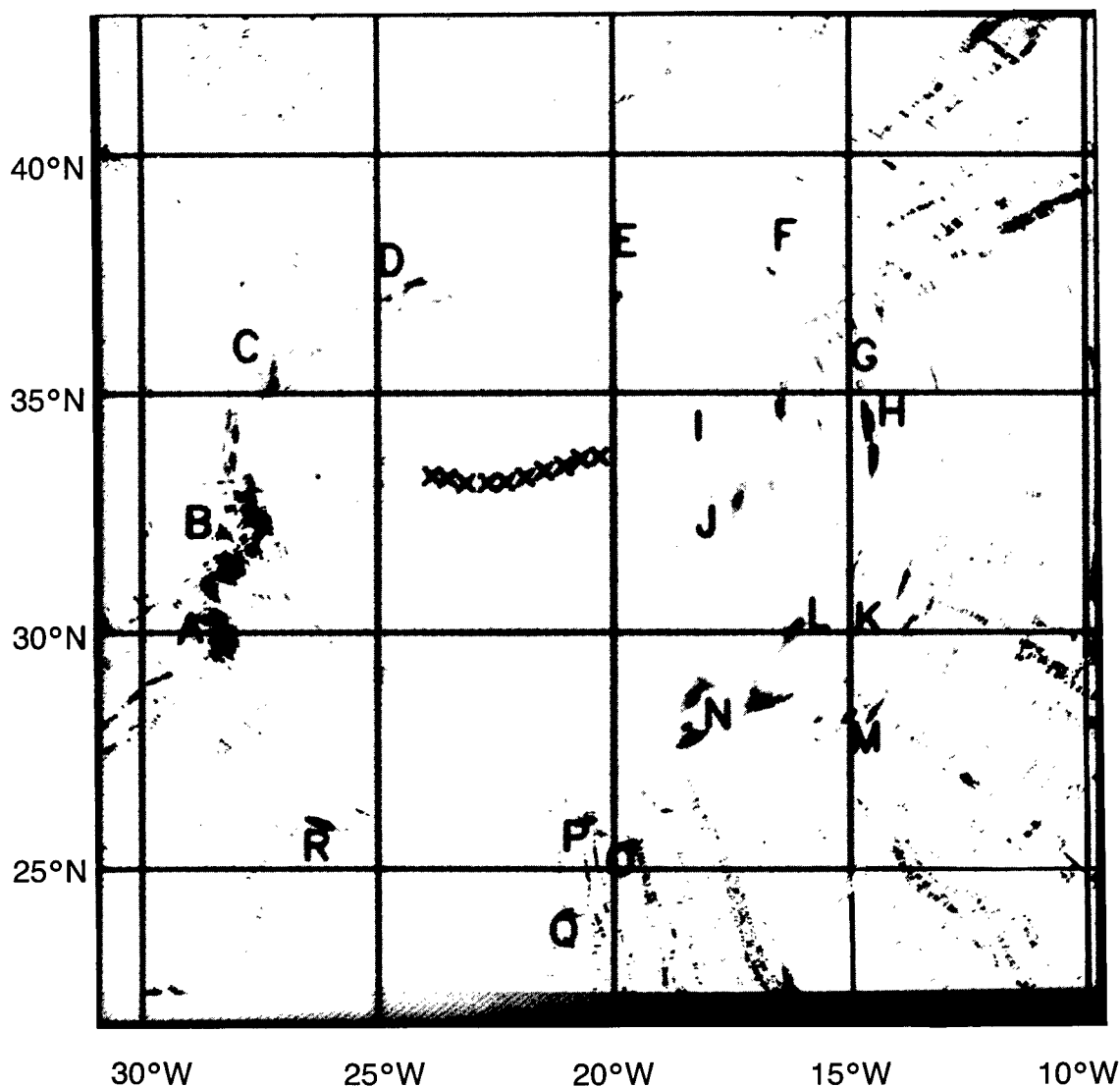
Fig. 8 — Integrated reverberation-bathymetry map for Canary Basin. Created by averaging single-shot maps for shots 10 through 19 as described in text. Map is 21° 20' on each side (about 2371 km north-south × 1988 km east-west). Each map pixel is about 1.'0 in size. Range of grayscale is from 6400 m (darkest) to 0 m (lightest).

From integrated reverberation-bathymetry maps like Fig. 8, we conclude that our long range reverberation mapping method is a success and that we are able to map all major undersea topography in a deep ocean basin with about a week of sea test time. We feel confident that with our technique it is possible to detect all major bathymetry (within perhaps 2000 m of the surface) in any deep ocean basin.

2.3 Confidence Estimates for Results

The third scientific objective in the analysis of BHST ocean bottom reverberation data is to give quantitative confidence estimates for our deduced seamount heights and locations. We now discuss these confidence estimates.

We have investigated the confidence that we can assign to our reverberation based estimates for topographic feature heights and locations (Sections 2.1 and 2.2). In our seamount height estimation

scheme, we have derived a functional dependence between the scattering strength measure, SS, and archival bathymetry heights and slopes. Although there may be some systematic errors in the calculation of SS vs range along each selected reverberation map radial, these errors are probably about the same for all radials. For example, a slight error in source level or backscattering area would contribute a slight bias up or down to SS. In transforming from the representation of Fig. 2 to that of Fig. 3, however, such a bias is removed.

Random errors, or nonsystematic errors, however, would result in a lower correlation coefficient and more spread of data points in Figs. 2 and 3. Such errors could arise, for example, in our estimates of reverberation power spectral density, or in our propagation loss estimates, or in the archival bathymetry that we use for comparison. Our reverberation levels have a one standard deviation uncertainty less than 3 dB. We estimate that the archival bathymetry heights are accurate to better than about ±500 m [Vogt et al., 1984]. To estimate the uncertainity in our propagation loss calculations, we ran the calculation with various estimates for first-cut bottom bathymetry, including a radial with archival bathymetry, another similar radial with one seamount removed and interpolated across, and another simple flat-bottom radial. These comparisons indicate that for our purposes the propagation loss result is fairly robust, i.e., the result varied by no more than ±3 dB over most ranges. Hence, we believe that the spread of points evident in Figs. 2 and 3 is mostly due to these random or nonsystematic errors, totaling perhaps ±6 to ±10 dB.

Another source of uncertainty is due to the fact that in our seamount height study, in some instances, we have chosen topographic features that lie on conjugate beam radials (see Sections 3.2, 3.3); however, our two-way propagation loss calculation was done only for the primary radials of interest. At near ranges (few hundred kilometers), the calculated propagation loss is probably adequate, but at greater ranges the calculated propagation loss may be off by 10 dB or more. These errors result in our height estimation uncertainty of about ±1.3 km at present. It may be possible to decrease this level of uncertainty by refinements in our analysis technique.

We are aware of the systematic offset between the range of our reverberation maxima and the actual bathymetry centroids (e.g., Fig. 6). This is expected, since the acoustic backscattering originates from the facing slopes of topographic features. This offset is on the order of 15 km and is dependent on feature height, being smaller for smaller topography. We have made no attempt in our current maps to correct for this systematic radial offset, although this could be done in future reverberation mapping studies. In our transformation from elapsed time for reverberation to topography range, we have used a constant nominal sound speed of 1500 m/s for simplicity. Actual sound speed may differ from this by about ±10 m/s at the time of our experiment and depends on position in the Canary Basin. We did not directly measure sound speed near the surface during the BHST experiment, nor did we attempt to use detailed estimates of archival sound speeds in our calculations of bathymetry range. We estimate that this simplification results in uncertainties in a range of up to about ±6 km. Our ship position was known to about ±2 km.

Another source of positional uncertainty is due to our reliance on magnetic sensors in the receiver array to determine receiver array bearings relative to true north. Although our receiver was capable of angular resolution finer than 1° in bearing, we had bearing uncertainties (after instantaneous correction for magnetic offsets between magnetic north vs true north) of about ±1°. This results in positional errors as great as about ±20 km on our single-shot maps, and likely results in some positional broadening on the integrated reverberation maps (Sections 2.2 and 3.4).

To summarize, random errors in our estimates of reverberation level, propagation loss, and archival bathymetry result in uncertainities in our estimates of seamount heights from reverberation data on the order of ±1.3 km. Bearing errors in our receiver result in azimuthal position errors for seamounts of up to about ±20 km. Our topographic range estimates are probably good to about ±6 km. These uncertainties could perhaps be reduced in future experiments by refinements in our technique.

3.0 FY 1982-84 BHST REVERBERATION DATA PROCESSING AND ANALYSIS

In Sections 3.1 through 3.4 we discuss in detail the processing and analysis procedures that we have developed from FY 1982 through FY 1984 for reverberation data from BHST. First, we discuss our laboratory-based software beamforming for improved receiver response. Then we discuss our processing to make a basin-wide reverberation map for each shot. We then discuss the analysis procedures for seamount height estimation using the reverberation maps. Finally, we discuss our analysis procedures for averaging single-shot maps together for a clearer picture of basin topography. For more details of our reverberation mapping FORTRAN software, we present a flowchart and program descriptions in Appendix B.

3.1 Software Beamforming for Improved Receiver Response

During the postexperimental transit phase of BHST the recorded hydrophone outputs were processed through the on-board time domain beamformer hardware. As described in BHST Report #2 [Schifter and Franchi, 1981], four iterations were required to form 256 beam outputs for each of the 34 shot returns. These beamformed reverberation levels represent received power spectral density vs azimuth from forward through broadside to aft relative to receiver tow direction. However, since the receiver array had approximately 40 inoperative ("dead") hydrophone groups, the sidelobe responses were considerably worse than optimal. For this reason, we developed software at NRL during FY 1982 to perform a phase and amplitude interpolation based on adjacent sensor outputs. This holefixing technique is described in detail by Schifter et al. [1985]. In addition, we developed software to perform frequency-domain beamforming on the hole-fixed data sets for each of the 34 shots to approximately 1 h after each shot detonation.

The laboratory processing of reverberation data on the HDDR tapes begins with two stages that we refer to as first pass and second pass processing. During first pass processing, the broadband time series for each shot detonation are read from HDDR tape and converted to hydrophone spectral time series by a fast Fourier transform (FFT) technique. During second pass, these hydrophone spectra are then processed by the holefixing software and then frequency-domain beamformed. The second pass beamformer outputs are saved as our "beam-time series" files for further analysis.

We expected that the revised processing at NRL would result in spatially resolved reverberation data with considerably lowered sidelobe responses, thus yielding higher reverberation to background levels and enabling us to search for smaller seamounts at greater range than would be possible in the time domain beamformed data set that had been processed during ship transit. To verify that this is the case, we have compared the outputs of the two beamforming techniques on the following types of signals: ambient background noise, including distant shipping noise; and backscattered acoustic returns from bathymetric features.

Figure 9 is a reverberation time history for one shot (number 12). We have averaged over a large number of beams (numbers 11 through 246) for purposes of this illustration. The ordinate is relative power and the abcissa is time frame number (where one frame represents a half-second average). Thus we have shown 750 s (12.5 min) of data in this figure. The arrows indicate times for injection of a sinusoidal calibration tone, typical ambient noise, and shot arrival respectively. In addition, we note the slight increases above ambient background at times near frames 1000, 1150, and 1325 corresponding to sea bottom convergence zone backscatter at about 56 km intervals. Figure 10 is a continuation of Fig. 9 for later times out to 2700 frames (corresponding to a range of 1013 km). The dashed curve in Figs. 9 and 10 is the output of the time domain beamformer. The solid curve is the output of the hole-fixed frequency domain beamformer (but offset by 10 dB for clarity). The large reverberation levels between frames 2050 and 2200 are due to backscattered acoustic energy from the Canary Islands.

Average Power per Beam
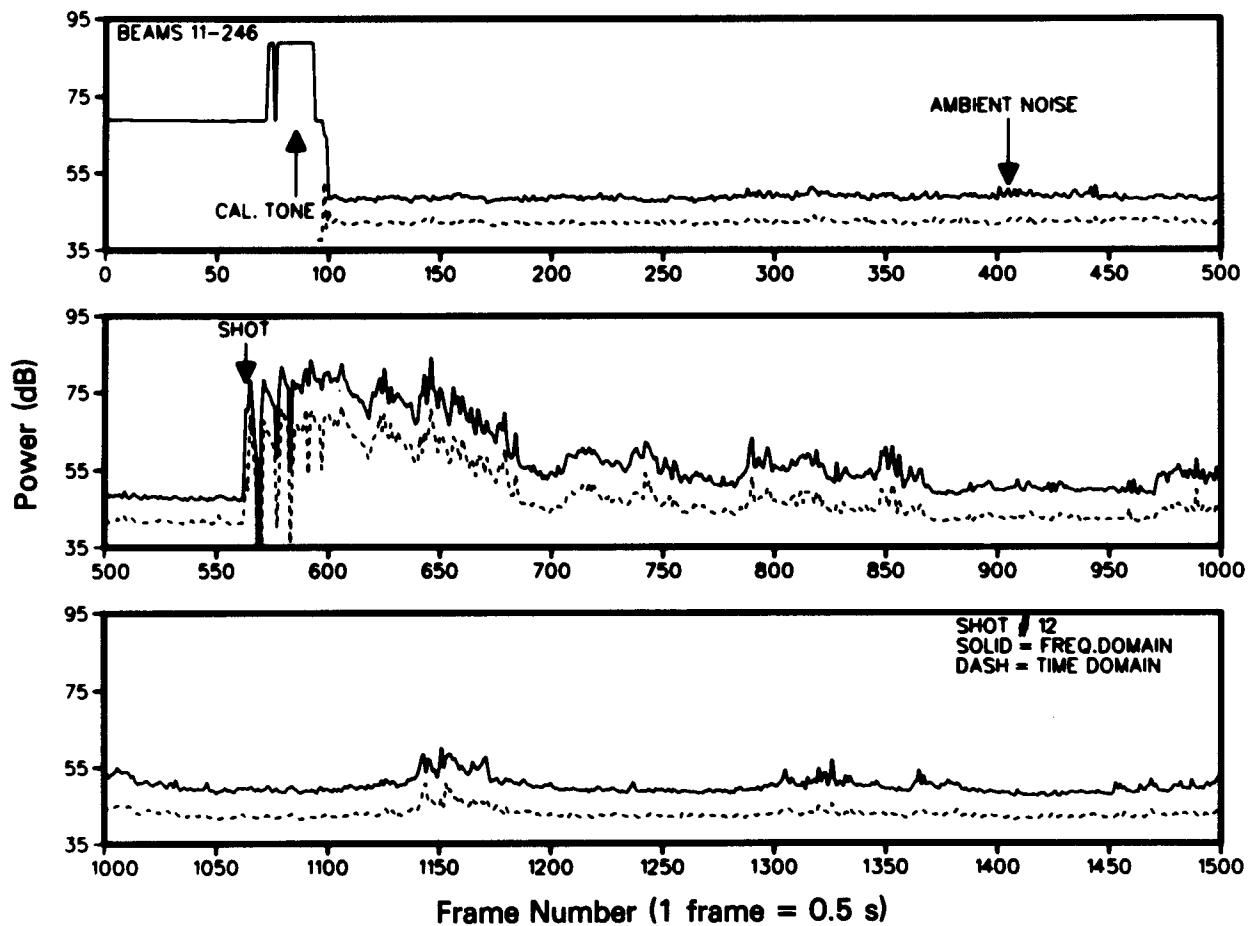

Fig. 9 — Receiver power spectral density vs time frame (1 frame = 0.5 s) for shot 12; averaged over beams 11 through 246 (Beam No. 1 = forward; No. 129 = broadside; No. 256 = approximately aft). Solid curve = frequency domain beamformer with holefixing; dashed curve = time domain beamformer (no holefixing). Curves are offset by 10 dB for clarity. Ordinate units: dB re 1 μ Pa^2/Hz.
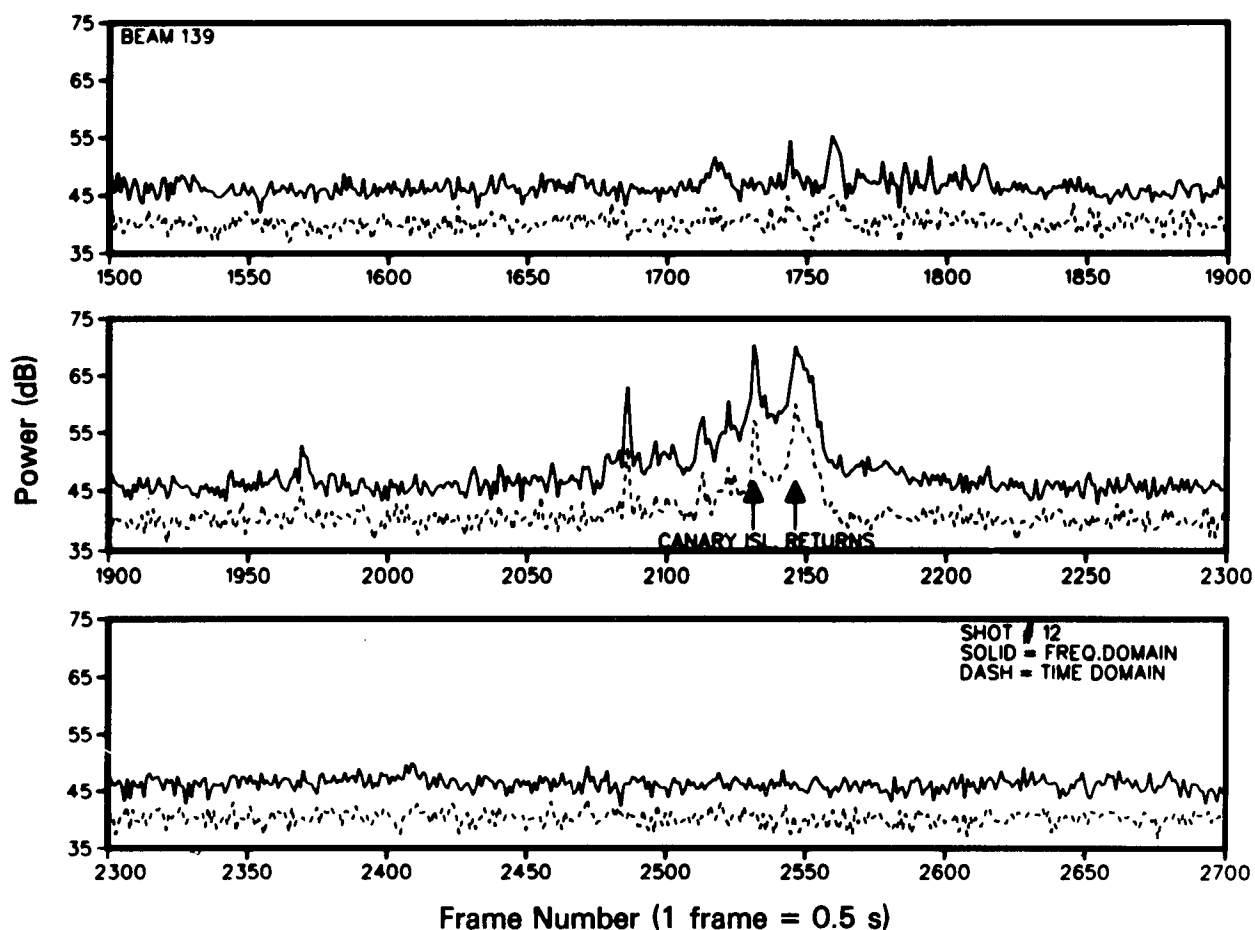
Average Power per Beam

Fig. 10 — Continuation of Fig. 9 but only one beam (No. 139; pointed toward Canary Islands)

To illustrate the improvement in signal to background noise, we have plotted in Fig. 11 the azimuthal distribution of received power for frame 405 of Figure 9 for both types of beamformers with no offset applied. We see the presence of distant shipping noise (e.g., bearings 115°, 125°, and 150°). The peak near bearing 14° is the direct arrival of own-towship noise. The peak near bearing 83° is own-towship noise reflected up from the bottom. The absolute levels of the distant shipping noise peaks agree to within about 1 dB, whereas the beams in between distant shipping are much quieter for the case of the frequency domain beamformer. The improvement in sidelobe quieting is about 5 to 7 dB in favor of the frequency domain technique. We have averaged over four frames (2 s) in each case. Figures 12 and 13 are similar to Fig. 11 except that we have deliberately chosen two times corresponding to acoustic reverberation from the Canary Islands (near broadside). Again we see a 5 to 7 dB improvement in signal to background level in favor of the frequency domain technique. The data of Figs. 9 through 13 have been averaged over a 60 Hz frequency band from 240 to 300 Hz.

We examine the beam-time data for any shot as a qualitative check on the beamformer output by using a program called PRESS.FOR (Appendix B). The output is displayed on our COMTAL color monitor device, and a hardcopy 8 × 10 in. Polaroid print can be made on our RAMTEK camera device. Figure 14 shows beam-time data for shot 12 with power spectral density represented by color (white = highest level, black = lowest level). The ordinate is time and the abscissa is bearing. Time runs downward in Fig. 14 with each subplot showing about 2 min of data (with slight overlap).

Comparison of Beamformers – Ambient noise

SOLID = FREQ. DOMAIN
DASH = TIME DOMAIN
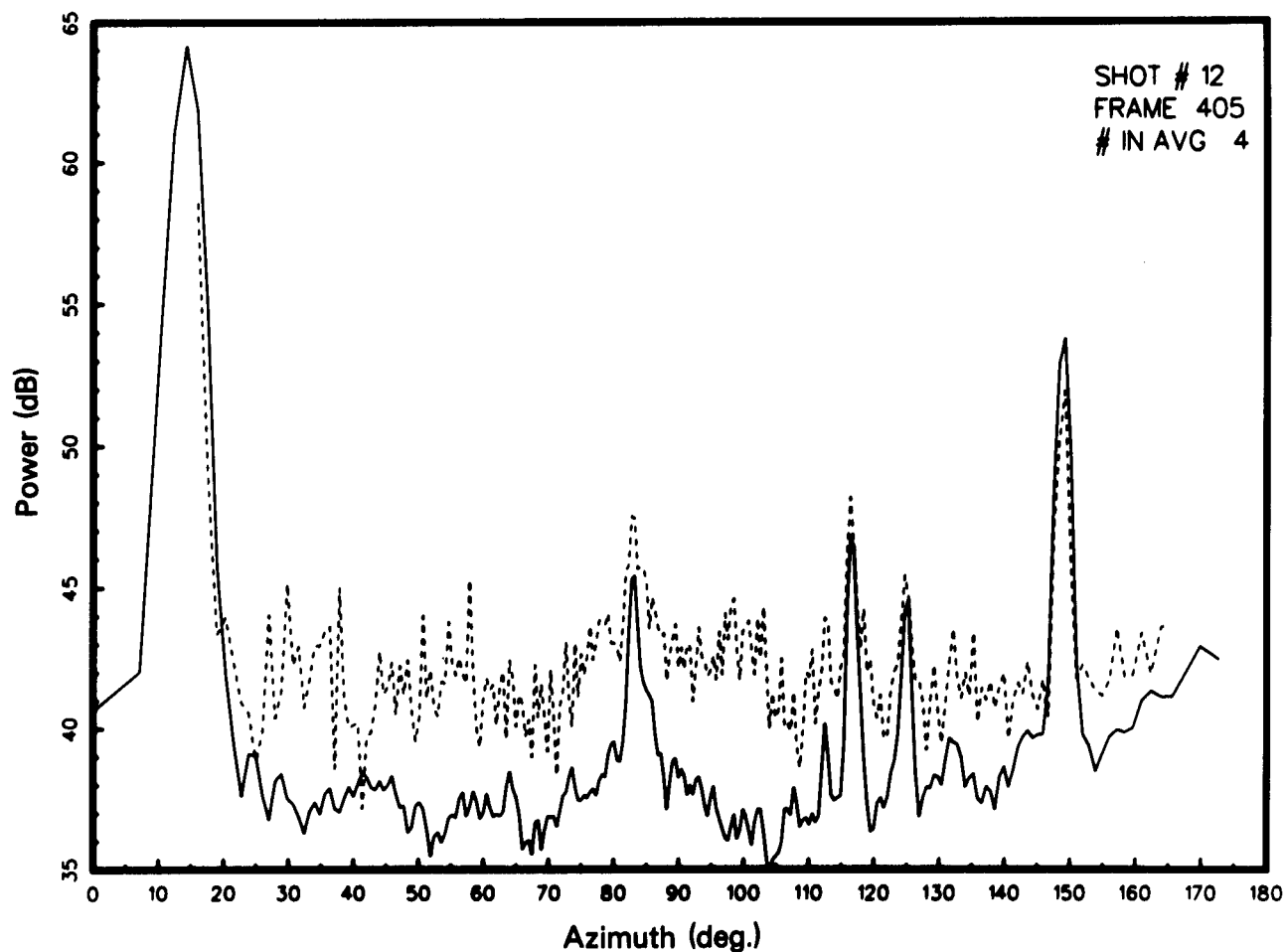
Fig. 11 — Received power spectral density (dB re 1 μ Pa^2/Hz) vs azimuth ($0°$ = forward, $180°$ = aft) for shot 12, and time frame 405 (average over 4 frames (2 s)). This is a plot of the azimuthal distribution of ambient noise corresponding to the time identified on Fig. 9. Solid curve—frequency domain beamformer (with holefixing). Dashed curve—time domain beamformer (no holefixing). There is no offset between the two curves. Note the reduced sidelobe levels for the frequency domain beamformer case.

Comparison of Beamformers – Return

SOLID = FREQ. DOMAIN
DASH = TIME DOMAIN

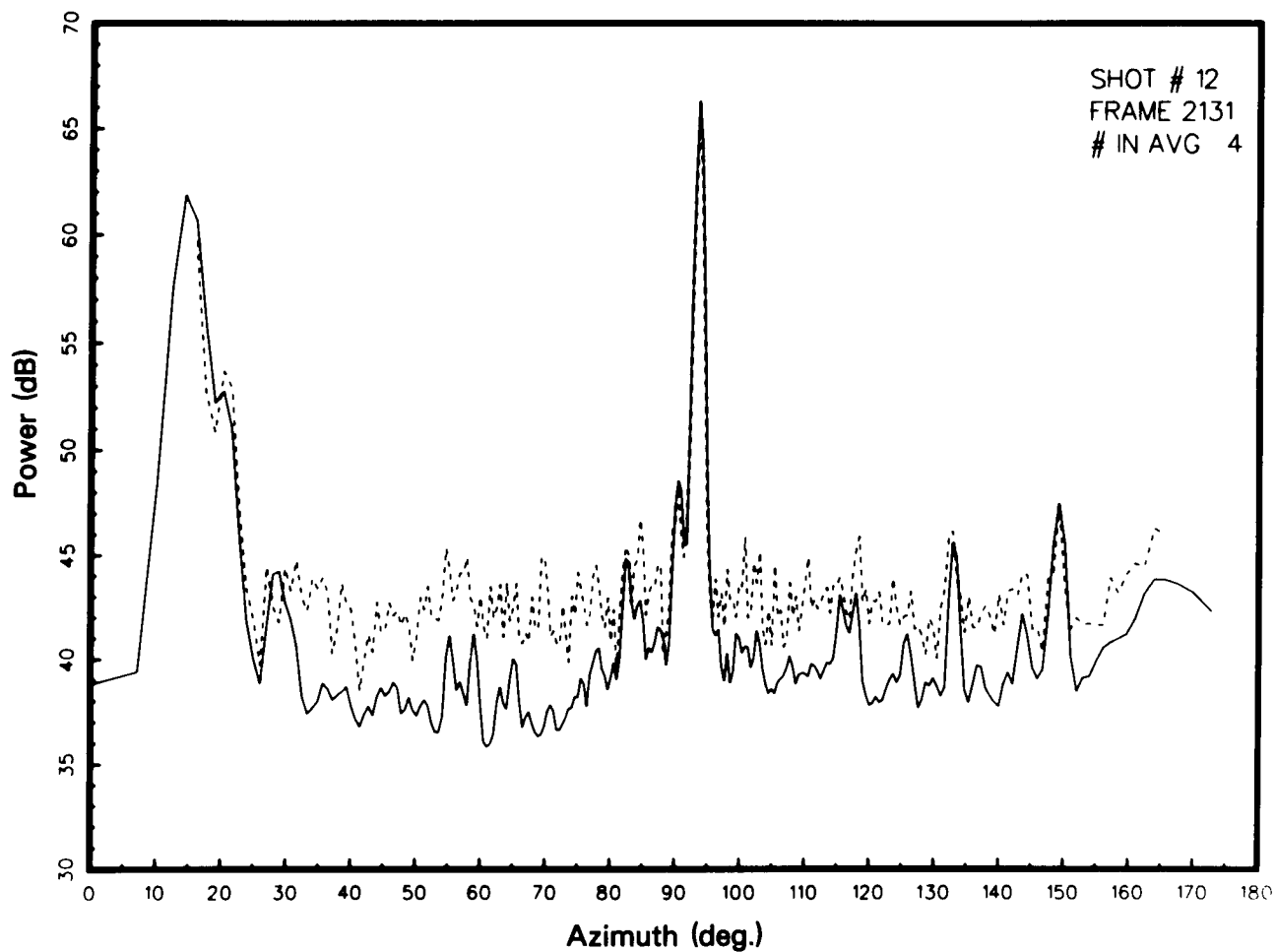Fig. 12 — Similar to Fig. 11, but for time of a return from the Canary Islands
(frame 2131; see Fig. 10)

Comparison of Beamformers — Return
SOLID = FREQ. DOMAIN
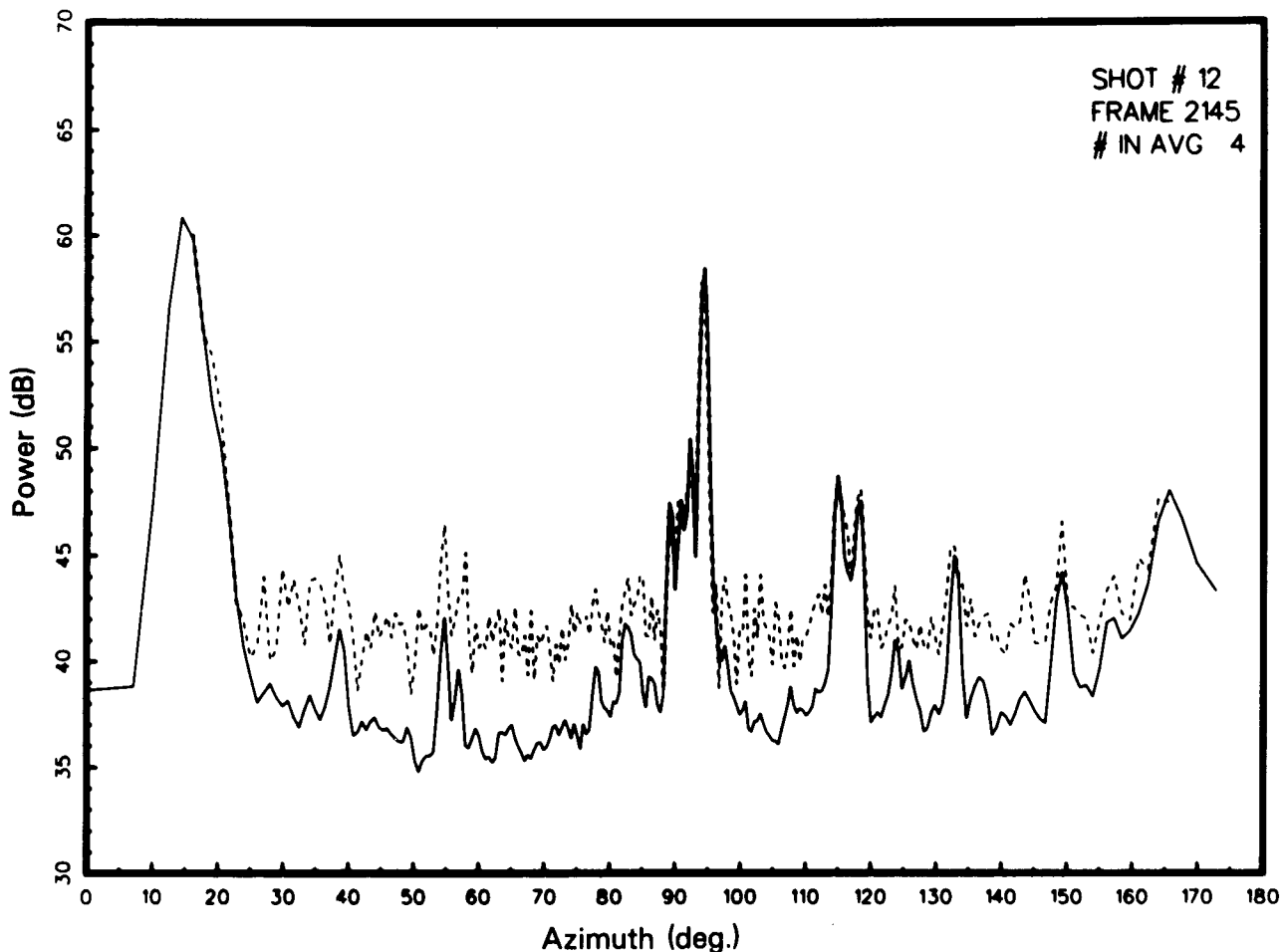### DASH = TIME DOMAIN

Fig. 13 — Similar to Figs. 11 and 12 but for time of another return from the Canary Islands (frame 2145; see Fig. 10)

Forward bearings are at left, broadside at center, and aft bearings appear at the right. Prior to shot detonation we see the quiet ambient background, which includes distant ship noise at several azimuths. For about a half minute after the shot detonation the bottom reverberation is very intense and the receiver electronics may be slightly saturated. The horizontal striations are high level returns caused by shot energy that has been reflected at high grazing angles from the sea bottom a,d surface, i.e., "fathometer returns." At later times, we begin to see distinct localized reverberant returns corresponding to discrete bathymetric features such as seamounts, as evidenced by the occasional bright patches at various bearings.

3.2 Single-Shot Reverberation Map Processing

The next step in our analysis of reverberation data is to transform the beamtime information for each shot into an actual two-dimensional reverberation map. To do this we use a program called NEWMAP.FOR (Appendix B). This program reads a beamtime file (BP**.DB), as well as timing information from file BHSTTIM.DAT and receiver position and heading information from file BHSTARR.DAT. Program NEWMAP then performs a transformation from beamtime format to latitude-longitude format.

Fig. 14 — Example of data in a beamtime format. This is received power spectral density (color coded); black—lowest, white—highest; each subplot is for about 2 minutes of data; there is slight overlap between the two subplots (see text for description).

17

Figure 15 shows an example of a single-shot reverberation level map in the latitude-longitude format. This map shows received power spectral density (color coded) for shot 12. The receiver array was being towed towards the southwest in this example. Since the receiver array is linear, each point in the beamtime file becomes transformed to two points in the single-shot map. There is a left-right ambiguity in the single-shot maps, hence for these maps we cannot resolve a backscattered return uniquely as being to the left or to the right of the receiver tow path. In Section 3.4 we discuss our map integration technique that enables us to resolve these spatial ambiguities. There are five basic types of acoustic signatures shown in the reverberation map of Fig. 15. They are:

- genuine backscattered returns from undersea bathymetric features such as seamounts (A),

- false images from bathymetric features that appear on the opposite side of the receiver towpath and that arise because of the left-right ambiguity effect (B),

- enhanced levels at sea bottom convergence zone ranges that appear as grainy concentric annuli (C),

- enhanced background in certain directions caused by distant shipping noise (D), and

- featureless ambient background noise (E).

We have omitted data for approximately the first half-minute during which the receiver electronics were recovering from the high levels caused by nearby bottom backscattering. FY 1982 processing concluded with the creation of a beamtime data file for each shot that we saved for further processing, and the production of a single-shot reverberation level map (polaroid print and digital data file) for each of the shot detonations.

3.3 Seamount Height Analysis Procedures

We have developed an analysis scheme for using the single-shot reverberation level maps (Section 3.2) to extract information about the sizes of bathymetric backscatterers. In Section 2.1 we summarized our scientific results from this remote method of obtaining seamount heights, and in this section we will discuss in more detail our analysis procedures.

The basic procedural steps in our seamount height estimation method are:

(a) Prepare a Synthesized Bathymetry (SYNBAPS) [VanWyckhouse, 1973] overlay (Fig. 16) for our single-shot color hardcopy reverberation level maps (e.g., Fig. 15). This SYNBAPS map shows bathymetry contours for the Canary Basin with 9.3 km resolution as well as the positions of individual shot detonations (at 4-h intervals).

(b) Examine all single-shot color reverberation maps for candidate seamounts, using the overlay of (a).

(c) For each reverberation map, prepare a list of potential great circle radials from shot position through candidate seamounts. Each radial is specified by shot position and initial bearing (as computed from positions of shot and seamount of interest).

(d) Choose a manageable subset of radials of interest from different shots (Fig. 16) (in this case, 32 radials from 12 shots). These radials are chosen to have seamounts at a variety of ranges from less than 200 km to about 1100 km at a variety of bearings relative to the
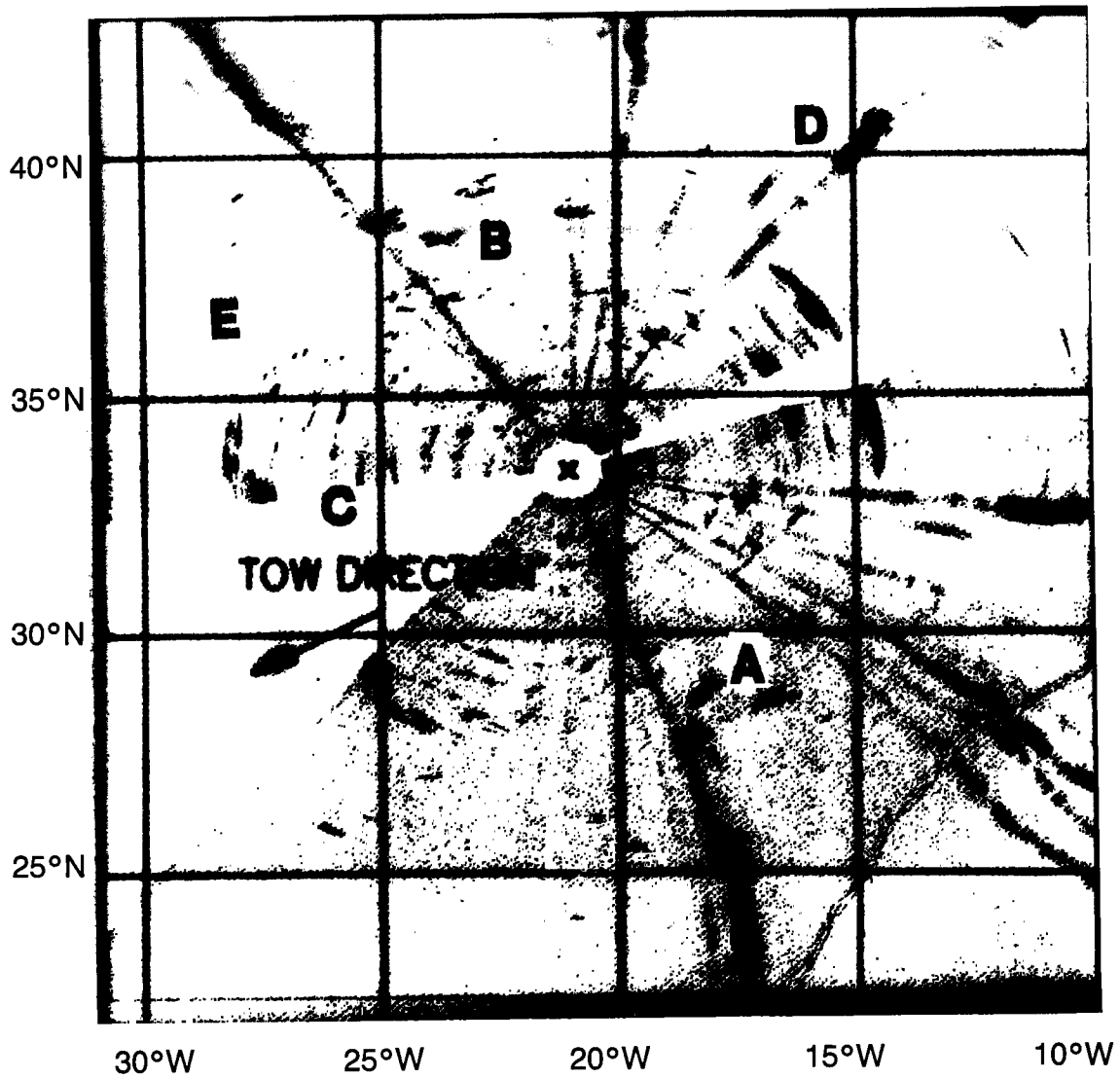
Fig. 15 — Single-shot reverberation level map (shot 12). Map is 21° 20' × 21° 20' (about 2371 km north-south × 1988 km east-west). Each map pixel is about 1.'0 in size. Range of grayscale is from 35 dB re 1 μ Pa²/Hz (lighest) to 65 dB re 1 μ Pa²/Hz (darkest). X denotes shot location. (For an explanation of the letter designations, see text.)
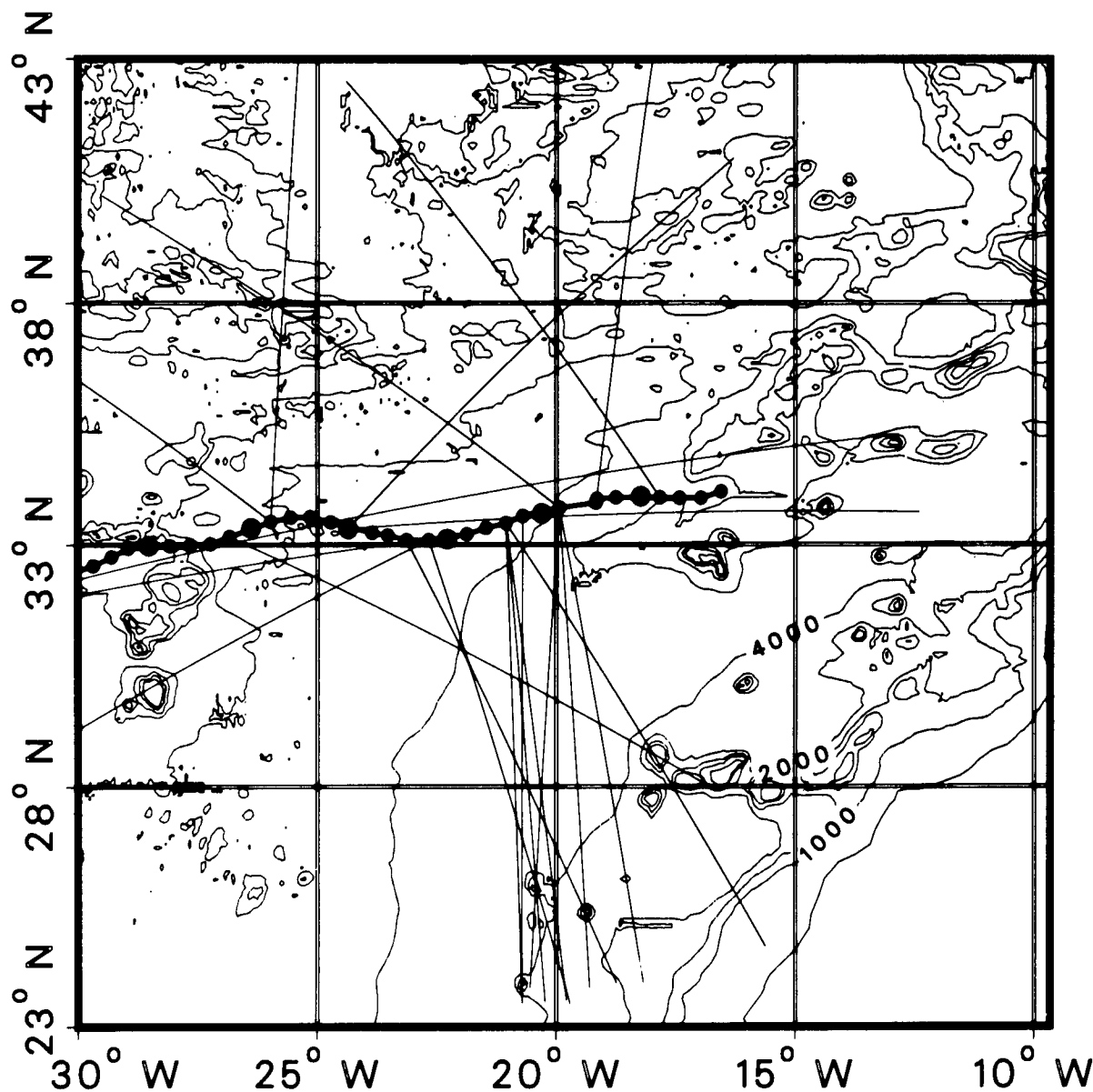
Fig. 16 — Map of SYNBAPS bathymetry for BHST op-area, showing track of ship (from east to west) and positions of shots (one every 4 hours). Also shown are great circle radials for seamount height study.

receiver array heading. It is not always possible to choose a bearing so that the reflected or conjugate receiver beam direction is looking down relatively flat bathymetry, although this is the case for about a third of the radials.

(e)   Run the NRL Reverberation Ray-Trace Model [Franchi et al., 1984] for each of the radials to compute two-way propagation loss. Inputs for the model are archival sound speed profiles and SYNBAPS bathymetry vs range and range-dependent bottom loss vs grazing angle estimates. Output is a data file for each radial containing the propagation loss vs range.

(f)   Run a FORTRAN program, which we developed, called REVBMSCAT.FOR. This program computes the following along each selected radial

$$SS = RLNET - SL + 2TL - AREA,$$

where:

$RLNET$ = 10 log (reverb level—ambient noise), in dB re 1μ Pa^2/Hz,

SL = source level, in dB re 1μ Pa^2/Hz,

$2TL$ = round-trip propagation loss estimate from (e), in dB, and

$AREA$ = geometric scattering area of an assumed flat bottom section of
ocean floor (in dB re 1 m^2); (no attempt to compute true seamount area).

Note that SS is a scattering strength measure, but not true scattering strength, because of the way we calculate the AREA term.

(g) Compile a list of the following for as many seamounts or other bathymetric features as possible from the subset of radials run in (f):

● Scattering strength measure, SS (record "peak" and "mean" (dB)),

● Range of SS "peak" (km),

● SYNBAPS bathymetry feature depth (km),

● Range of SYNBAPS feature peak (km),

● SYNBAPS bathymetry feature slope (deg).

(h) Perform a least squares correlation analysis to look for correlation between SS and SYN-BAPS bathymetric feature heights and slopes. Derive the "functional dependence" of SS on seamount height and seamount slope (see Section 2.1).

(i) Apply the functional dependence derived in (h) to a composite backscattering strength map that we will create using the procedures to be discussed in Section 3.4, to make a reverberation-based, basin-wide ocean topography map of the Canary Basin (see Section 2.2).

The program REVBMSCAT (step (f) above) has as its main objective the calculation of "scattering strength measure" vs range along a selected radial. This program outputs a sequence of seven plots of information related to a particular radial. We show a typical example of a set of these plots as Figs. 17 to 23.
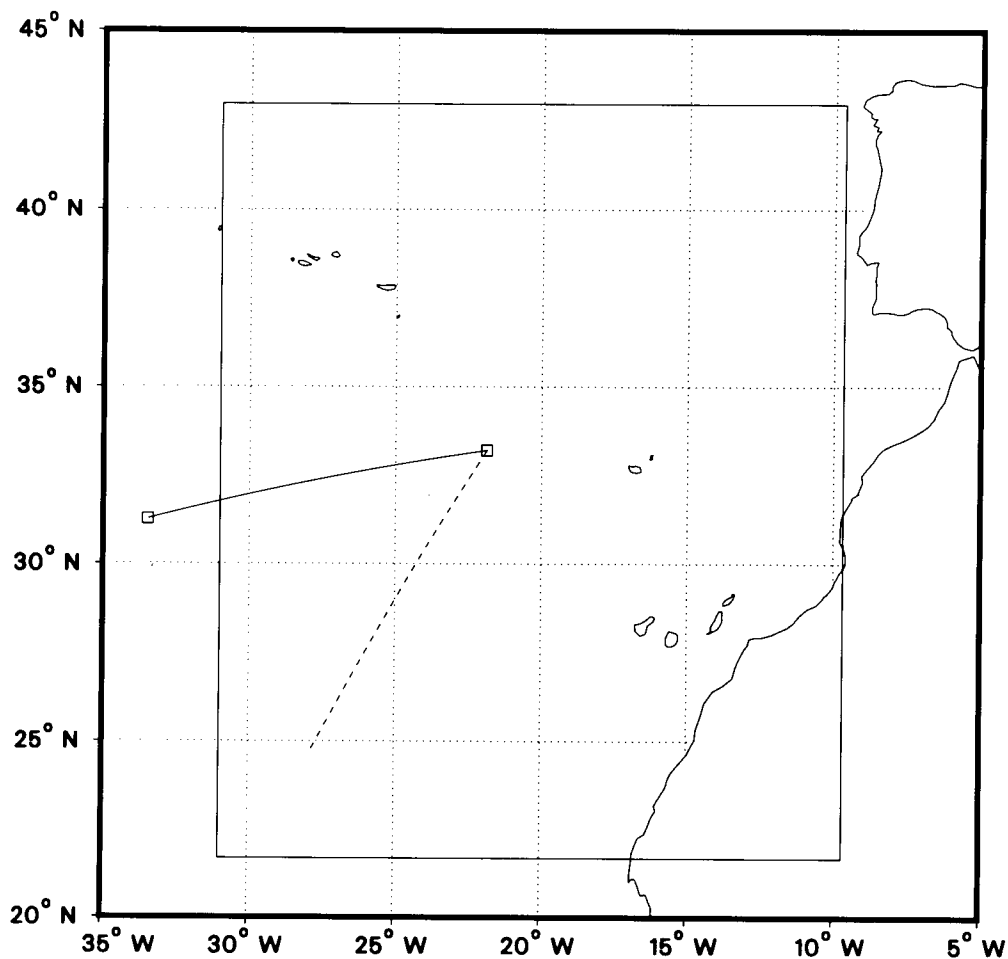
OUTLINED AREA IS REGION COVERED BY BHST MAPS

SOLID LINE LEAVES SHOT 14 LOCATION AT BEARING 261.90 DEGREES

DOTTED LINE IS REFLECTION ACROSS ARRAY

RADIAL NO. 1

Fig. 17 — Sample plot from program REVBMSCAT. This plot shows map of BHST op-area with a seamount height study radial (solid curve) and its conjugate beam radial (dashed). Receiver array was headed southwest. Area enclosed by inner box is 21° 20' north-south × 21° 20' east-west region of our BHST digital map files. This example is for shot 14; primary radial at bearing of 261.94°

BEAM POWER vs TIME
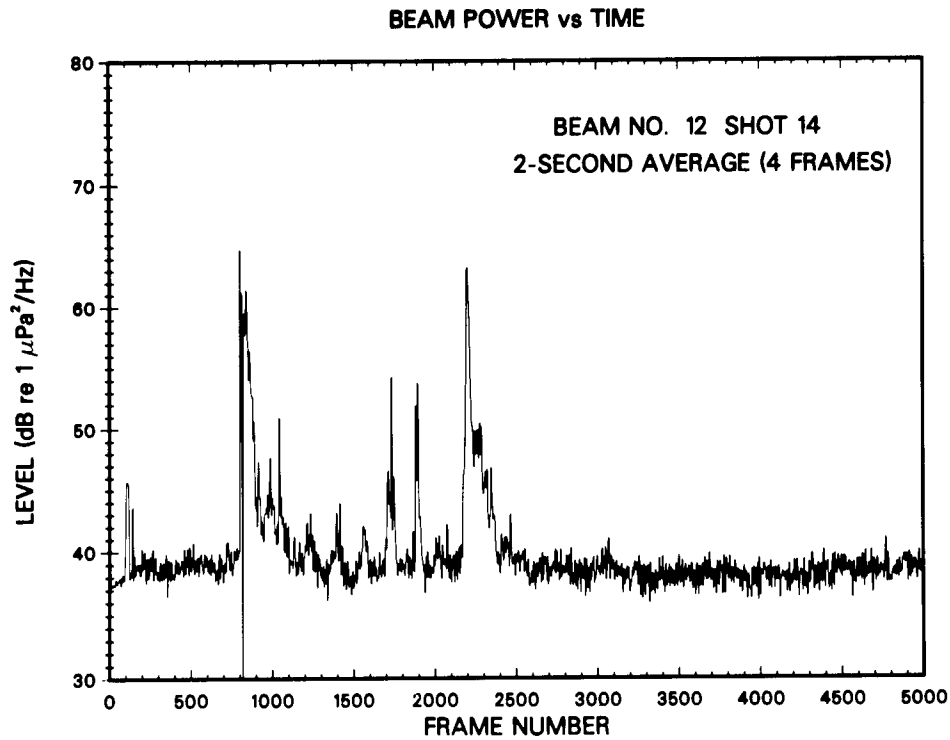
Fig. 18 — Sample plot from program REVBMSCAT. This plot shows received power spectral density vs time frame from our digital beamtime file BP14.DB for shot 14, beam No. 12. Data are averaged over four frames (2 s). Small signal near frame 100 is a calibration tone; large signal near frame 800 is direct arrival of shot; later returns are due to ocean bottom reverberation. Ordinate units are dB re 1 μ Pa^2/Hz.
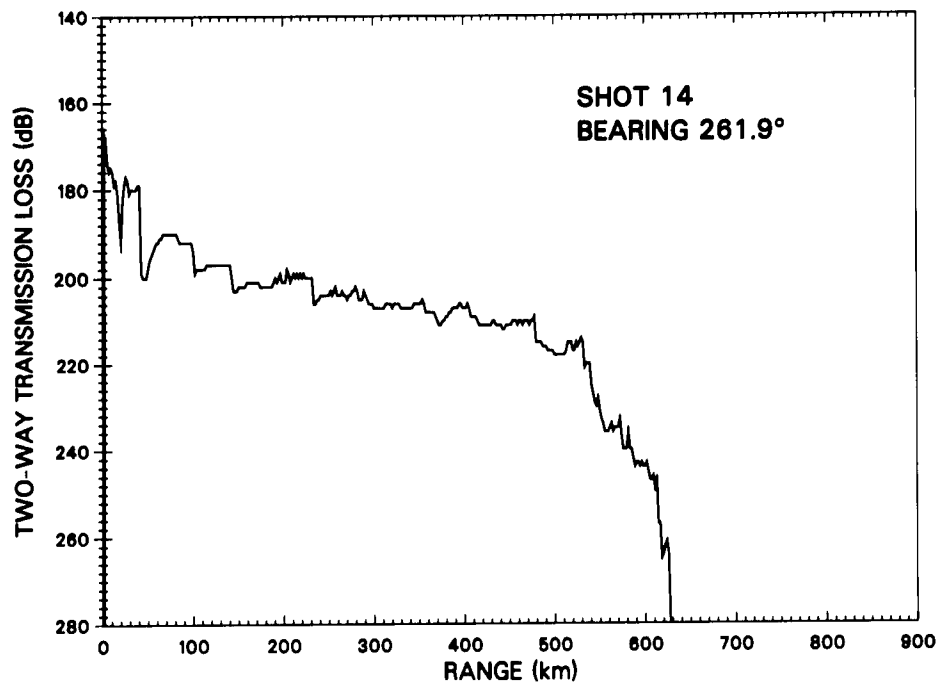
Fig. 19 — Sample plot from program REVBMSCAT. This plot shows two-way propagation loss computed using the NRL Reverberation Model, NREV-1 for the primary radial of Fig. 17.
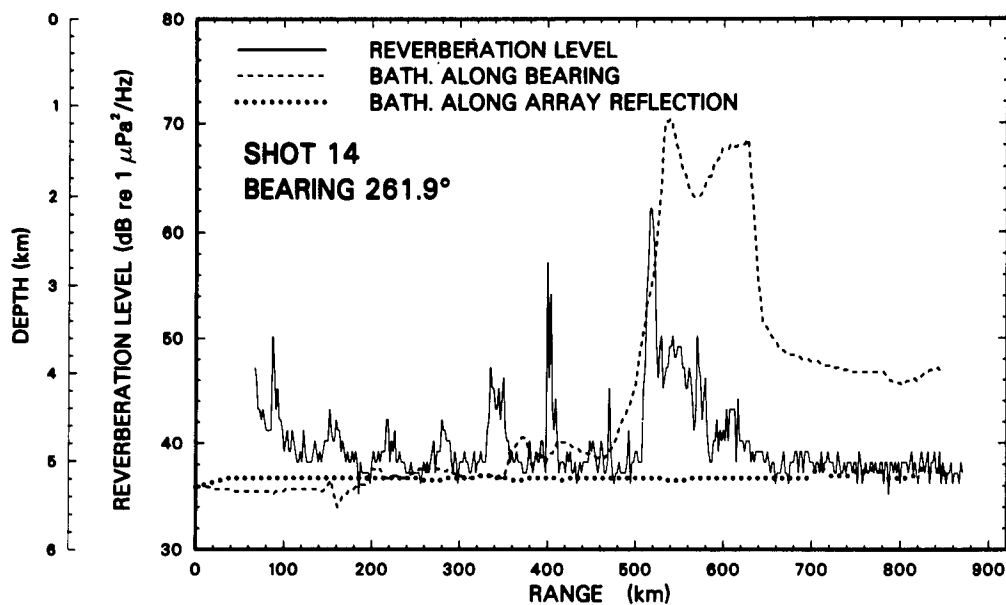
Fig. 20 — Sample plot from program REVBMSCAT. This plot shows reverberation power spectral density (dB re 1 μ Pa^2/Hz) vs range along primary radial of Fig. 19 from our digital map file MP12.DB. Slight differences between this curve and that of Fig. 19 are due to the fact that this great circle radial may span more than one beam as it goes out in range; and our reverberation levels are converted to integer byte format for compatibility with our COMTAL image monitor. Near range bottom reverberation (inside of about 65 km) is omitted from our single-shot map files, hence the short gap at left. Also superimposed to same range scale is SYNBAPS bathymetry for primary radial (dashed) and conjugate radial (dotted).
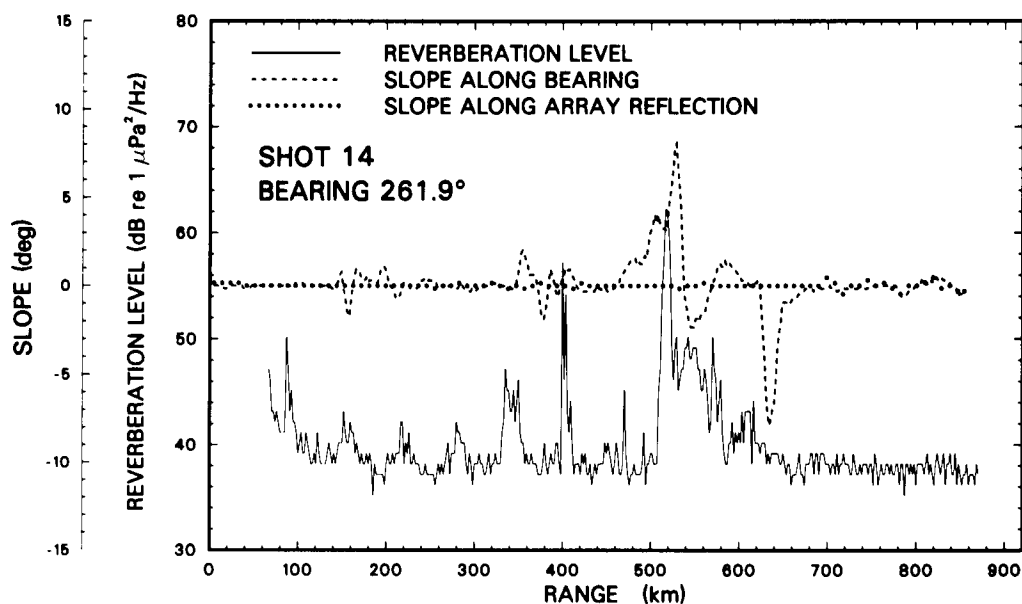
Fig. 21 — Sample plot from program REVBMSCAT. Similar to Fig. 20, but with SYNBAPS bathymetric slopes instead of depths.
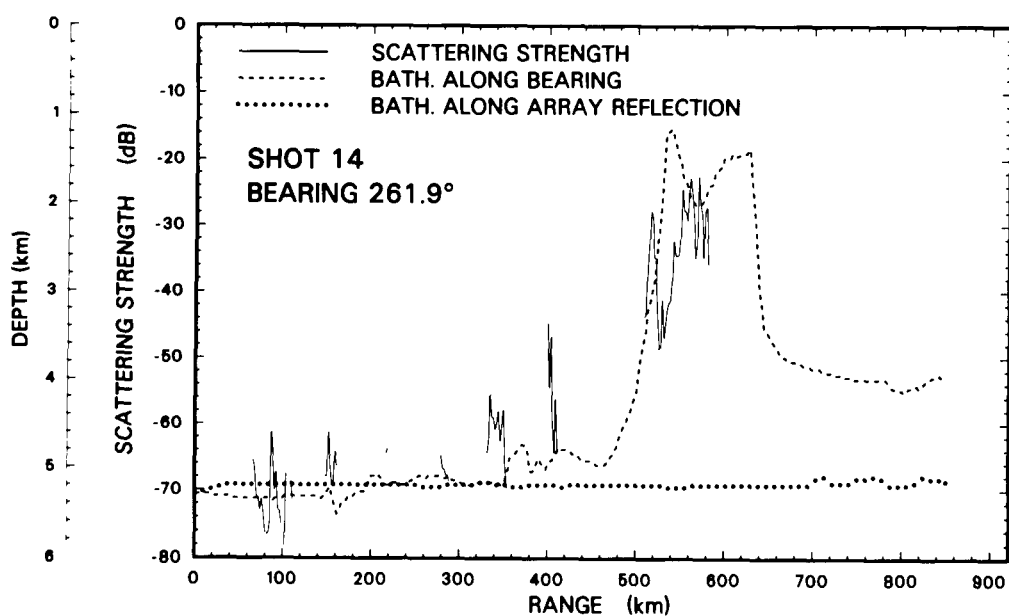
Fig. 22 — Sample plot from program REVBMSCAT. Scattering strength measure (see text) vs range (solid curve) for a selected radial. (Note, the curve is not continuous because scattering strength is only computed for ranges where the reverberation level is above the background noise level by a chosen threshold value, e.g., 3 dB.) Also shown is SYNBAPS bathymetry for primary radial (dashed) and conjugate radial (dotted) of Fig. 19.

Fig. 23 — Sample plot from program REVBMSCAT. Similar to Fig. 22, but with SYNBAPS bathymetry slopes instead of depths.

We describe these seven plots briefly (example is for shot 14). Figure 17 is a geographic map showing the location of the shot and the great circle radial corresponding to the primary bathymetry of interest (solid) and the great circle radial corresponding to the ambiguous conjugate receiver beam direction (dashed curve);
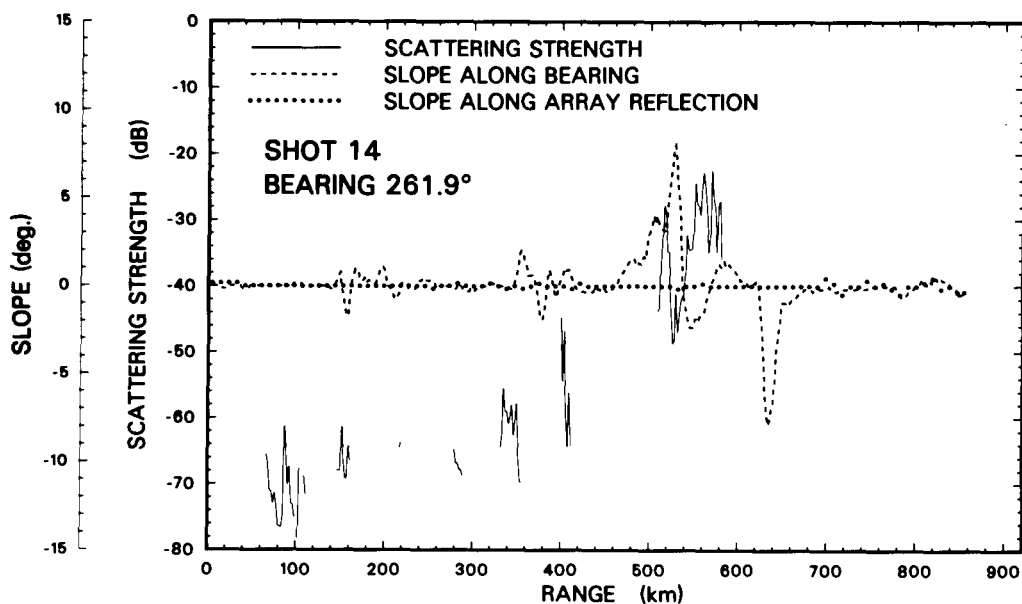
- Fig. 18 shows received level vs time for beam direction of interest, from the digital beam-time file used to estimate ambient background level before shot direct arrival; 1 frame = 0.5 s;

- Fig. 19 shows the two-way propagation loss vs range from the NRL Reverberation Model;

- Fig. 20 shows received level vs range (time) looking along the primary great circle radial in the digital single-shot .reverberation map file for this shot; as well as SYNBAPS archival bathymetry along this same radial (dashed) and along the conjugate radial (dotted);

- Fig. 21 shows received level as in previous figure, but with SYNBAPS bathymetry slopes instead of heights;

- Fig. 22 shows "scattering strength measure" vs range (time), as well as SYNBAPS bathymetry as in Fig. 20; and

- Fig. 23 "scattering strength measure" vs range (time), as well as SYNBAPS bathymetry slopes as in Fig. 21.

The plots described above are used to tabulate the various quantities for the correlation analysis in our seamount height study (Section 2.1).

3.4 Map Integration Procedures for Imaging Bathymetry

In this section we discuss the analysis steps for averaging single-shot reverberation maps together to image undersea topography. We have developed a sequence of FORTRAN programs to

- create range-independent two-dimensional backscattering strength maps from our single-shot reverberation beam-time files;

- combine single-shot results into a cumulative map, and

- apply a spatial filter to the cumulative map.

These programs make practical use of the information present in the reverberation data, including known properties of the signals and noise. Ideally, we would like all of the decisions in the processing sequence to be made automatically; therefore, a second goal for these programs is to reduce required user interaction to a minimum.

In Appendix B we give a flowchart of the various programs and files, and their interdependence in a typical processing run. The double asterisk (**) in file names stands for the number of the particular shot being processed. We now describe our analysis for converting received reverberation to a range-independent "scattering strength" map for each shot. Next we discuss our analysis to combine single-shot maps for an improved basin-wide map of major acoustic scattering topography.

3.4.1 *Conversion from Directional Received Level to Directional Backscattering Strength*

The directional reverberation levels in our beamtime (BP**.DB) files are converted for each of 256 receiver bearings to directional scattering strengths by using

$$SS = [RL - NL] - SL + 2TL - AREA,$$

where

SS = ocean bottom "backscattering strength" (dB re 1 m (dBm))

RL = measured beam level (dB re $1\mu Pa^2/Hz$),

NL = directional ambient noise level (see below),

SL = source level (dB re $1\mu Pa^2/Hz$),

2TL = two-way propagation loss (dB),

$$AREA = 10 \log (\theta\ rdr) = 10 \log (\theta\ c^2\ t\ dt\ /4),$$

and the [ ] denotes a linear subtraction (not in dB). The source level is known, and the area term is easily calculated using t = elapsed time since shot detonation (s), and dt = averaging interval (2 s).

We now discuss the determination of the background noise and propagation loss terms in some detail.

Background Noise Level Estimation and Subtraction

The actual ambient noise level (including shipping noise) is some partially random function $A(\theta,t)$ that we wish to estimate as well as possible by some function NL (θ,t). The goal is to minimize var $(A(\theta,t)$-NL $(\theta,t))$.

The first step in estimating A is to note that the mean noise level varies from beam to beam because of differing beam widths and shipping noise. Recordings of ambient noise from before the shot detonation (therefore free of reverberation) are averaged over time to give NL (θ), the mean noise level for each beam.

The second step in estimating A is to observe that temporal variations in ambient noise levels appear to be correlated from beam to beam; that is, cov $(A(\theta 1,t), A(\theta 2,t)) > 0$. A least part of the variation in the noise levels on the beams appears to be in the form of a uniform omnidirectional fluctuation that could be caused by flow noise or other near-field effects. If an omnidirectional noise level NL(t) can be found at an arbitrary time t, then the variations in this level can be used to better estimate $A(\theta,t)$. We assume that NL(θ,t) = NL(θ) + NL(t) since distant ship noise and array flow noise should be independent. We expect

$$var (A(\theta,t) - ML(\theta) - NL(t))$$

$$< var (A(\theta,t) - NL(\theta))$$

$$< var (A(\theta,t)).$$

28

The omnidirectional noise level NL(t) for a given time frame is in practice estimated by taking the 25th percentile of the distribution of reverberation levels on beams 11 to 250. This method is less sensitive to reverberation than a simple mean would be (returns imply that RL(θ,t) is unequal to A(θ,t)). It is still important, however, that most of the beams in a given frame contain only ambient noise, and not returns (signal), or else this method will fail. In general, the only times when most beams contain signal are immediately after the shot and in convergence zones. Temporal adjustment of NL is done only after a user-specified interval past detonation.

Determination of Two-way Propagation Loss in the Ocean

As a starting point for transmission loss (TL) vs range estimates, a monotonically increasing, smooth TL curve was fit to sample calculated transmission loss from runs of the NRL Reverberation Ray Trace Model [Franchi et al., 1984]. These model runs were performed by tracing rays from source and receiver depths to a nominal depth of 4000 m, chosen as a characteristic seamount depth, although the result was fairly insensitive to the exact depth chosen. Departures from our calculated smooth curve are rather site dependent, so we decided not to use the ray trace model to produce any more complicated transmission loss function. We wanted a relatively site independent result for TL so that we could use the same TL for a given shot along all bearings.

The actual transmission loss is not monotonic, as evidenced by the presence of convergence zone rings on the reverberation level maps. We attempt to have the software detect these convergence zones and incorporate them into the transmission loss. This is done as follows: for each time frame, we find the 25th percentile of the distribution of reverberation levels on beams 11 to 250 (the same as for noise levels, above). We assume that this reverberation level is that which results from scattering from a bottom with a fixed typical scattering strength. In other words, we are assuming that TL is azimuthally isotropic, and that the terrian being surveyed is essentially flat and featureless, with few beams containing topographic features (i.e., seamounts) at any given time (this assumption will not hold for shots in the midst of seamounts).

We then calculate transmission loss with program GETTL.FOR (Appendix B), using this reverberation level according to

$$2TL = -[RL0-NL] + SL + SS0 + AREA,$$

where SS0 is the nominal bottom backscattering strength assigned to the typical bottom, and RL0 is the omnidirectional reverb level found above. In Fig. 24 we show an example of two-way transmission loss as determined in this manner.

With sufficiently low noise level, this method could be used to find transmission loss at all times; in practice, however, we must have a good signal-to-noise ratio to estimate TL from this formula in any reasonable manner. The NL used here is the omnidirectional noise level determined before the shot. Problems usually appear in the form of noise level fluctuations, which damage this estimate of TL. High-frequency noise can be eliminated by smoothing, but low frequency changes in overall noise level often throw off this algorithm, since in practice RL0 differs from NL by less than 1 dB for many regions of interest. Note that calculation of TL from reverberation data requires that the typical beam have signal content, whereas temporal adjustment of noise levels requires that the typical beam have very low signal content; hence the TL adjustment algorithm and noise adjustment algorithm cannot both work at any given time (i.e., they are applied at separate times).

Because of background noise fluctuations, the output of the program GETTL must be checked by the user. If the resulting TL curve appears anomalous, then the user must specify the noise level, overriding the default selection. The program GETTL could be improved if we could devise a good
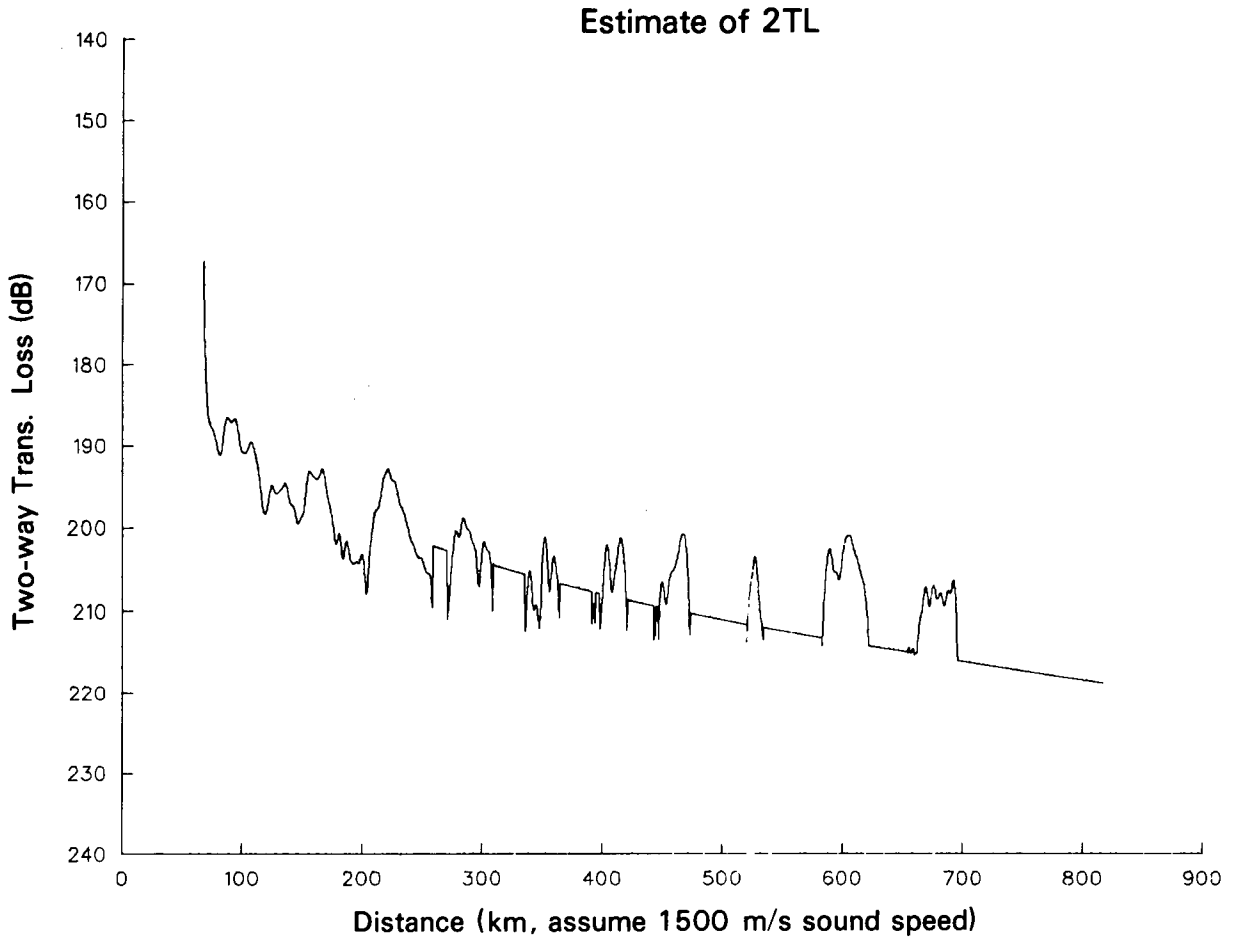
Fig. 24 — Sample plot from program GETTL. Two-way transmission loss vs range estimate for shot 12; used for creating a single-shot scattering strength beam-time file SS12.DB with program SS (see text and Appendix B).

way to distinguish low-frequency noise level fluctuations from convergence zones in the reverberation data (usually one can tell by eye from the reverberation maps). In general, we are able to set a threshold distinguish between the two cases.

This step in our procedures helps reduce the convergence zone "rings" (e.g., section 3.2, Fig. 15) at the outset before we average our single-shot maps together (section 3.4.2).

Noise Thresholding and Minimum Detectable SS

Because of the variability in ambient noise, we must assign a threshold (lower limit) to RL below which the signal level computed by means of [RL − NL] is unreliable. A single beamtime element is considered to contain signal if [RL − NL] > 3 dB (s/n > 1), and to contain only noise if [RL − NL] < 3 dB (s/n < 1).

For those points marked as noise, we wish to use the fact that the signal was undetectable. To this end, a minimum detectable scattering strength SS_{min} is calculated for these points by using

$$SS_{min} = NL - SL + 2TL - AREA.$$

When we later average maps together, we make use of the concept that SS $\leq$ SS$_{min}$ at a "noise" pixel. Two effects can invalidate this concept, acoustic shadowing by topographic features and loud shipping noise. We now discuss these effects and our efforts to recognize and deal with them:

Shadowing—If two seamounts happen to lie close to each other along the great circle radial from which shot energy is received, then the seamount nearest to the sound source may acoustically shadow the one behind it. In accounting for shadowing, we use the concept that the sound energy incident on a seamount is subject to one of three outcomes

- backscattering,

- forward scattering, or

- absorption.

In general, the first of these is small compared to the second and third. We can express the fraction of incident sound energy corresponding to these three as f_r = reflected (backscattered), f_t = transmitted, f_a = absorbed; and $f_r + f_t + f_a = 1$. We solve for a shadowing factor, f_t, the fraction of energy transmitted (available for later backscatter) as $f_t = 1 - (f_r + f_a)$ by making rough estimates for f_r and f_a at each seamount encounter ($f_t = 1$ corresponds to "no shadowing").

We developed a preliminary algorithm to keep track of the cumulative effects of shadowing on each beam. If potential shadowing on any beam rises above a certain level, then all subsequent noise frames on that beam have SS$_{min}$ set to zero (dB). This means in effect that no information is extracted from shadowed pixels.

We would like to have a more rigorous shadowing algorithm that adjusts transmission loss to account for blockage by topography. A fundamental obstacle to this is the left-right ambiguity effect that makes it uncertain whether two reverberation signatures on the same beam are actually responses to topography along the same great circle radial or along different radials corresponding to the main beam and conjugate beam directions. In practice, we seldom used our present shadowing algorithm because of the difficulties mentioned above, but we consider this to be a starting point for further algorithm development.

Detection of Strong Shipping Noise—Distinguishing shipping noise from returns is a relatively simple task for the eye and brain, but is difficult to get the computer to do. When doing this by eye, we look for roughly contiguous radial tracks on the maps; to get the computer to do this on the full data set would be difficult, given the large amount of data present. Deletion of shipping noise is very important, since if left in the maps it will be mistaken for very strong scatterers (especially at large distances), making it difficult to average down.

We have developed a semiautomated method to identify shipping noise in our data. As a first step, for each beam we examine blocks of 200 time frames (100 s). Of these 200 reverberation levels, the 60th largest is taken to be a representative noise level for that beam over that 100-s time period. A small correction for varying beamwidths is also applied. This 30th percentile measure is useful for several reasons, first, it begins the search for long contiguous tracks of high reverb levels, because a short (i.e., 5 s) return in a 100-s data sample will not alter the 30th percentile very much. Only shipping noise, a large return, or a series of returns on the same beam will cause this 30th percentile to rise substantially above the natural noise level. Second, taking 200 time frames greatly reduces random noise fluctuations. Third, this 200-fold reduction in the amount of data makes further intelligent processing much more feasible.

The first step, discussed above, produces a reduced beam-time file, MD**.DB (see Appendix B). Figure 25 is an example of a map file that was made from such a MD**.DB file with program NEWMAP and displayed with program APDIS, as a graphic aid to the user in identifying shipping noise. The bright radial "tracks" are portions of the map that contain shipping noise.

The second step is a simple thresholding scheme. Any element of the MD**.DB file that is above a user-selected threshold is marked as shipping noise. The third step is the identification of all distinct contiguous regions of marked data (all separate tracks). Regions that span more than a preselected time period are marked as shipping noise. Those regions that are shorter are considered to be good data (which would have been misidentified by simple thresholding). The fourth step is interactive; the user may change the identification (shipping/good data) of any region or any single beam-time element in the MD**.DB file.

If an element in the MD**.DB beam-time file ends up marked as shipping noise, then the data from each of the 200 corresponding points in the original BP**.DB beam-time file is ignored.

The program ZONE is the main algorithm for shipping noise detection and deletion. It allows us to detect any radially extended shipping noise on our maps. However, the user must still interact with the program to check all of its automatic shipping noise assignments. We could develop more advanced algorithms using the concept that shipping noise is louder on a given beam than on neighboring beams, rather than just above a fixed threshold. However, some kind of user check may always be necessary, and excessive numbers of user decisions are inefficient and can lead to difficulties because of user biases (i.e., knowing where seamounts are supposed to be). It may eventually be necessary to return to the complete beam-time file, rather than the condensed MD**.DB file, if a really user-independent algorithm is to be made, because not even the eye can completely distinguish shipping from signal on the maps made from MD**.DB.

Single-Shot Scattering Strength Map Files—In summary, for each point in the beam-time file BP**.DB, the following is done

- calculate the background noise level (ambient beam level, with possible temporal correction)

- determine 2TL at this range (from ray-trace results or from examining reverberation levels)

- label the point as signal or noise, depending upon [RL − NL]

- —if this is signal, calculate SS

  —if this is noise, calculate SS_{min}.

Sets of four 0.5-s frames are then averaged into 2-s frames to be compatible with program NEWMAP. A reverberation level frame is labeled as signal if two or more of the input frames are signal. The output "beam-time" formatted file (SS*.DB) then takes on the following values

SS if the point is signal (dBm)

−SS_{min} if the point is noise (these values are hence > 0)

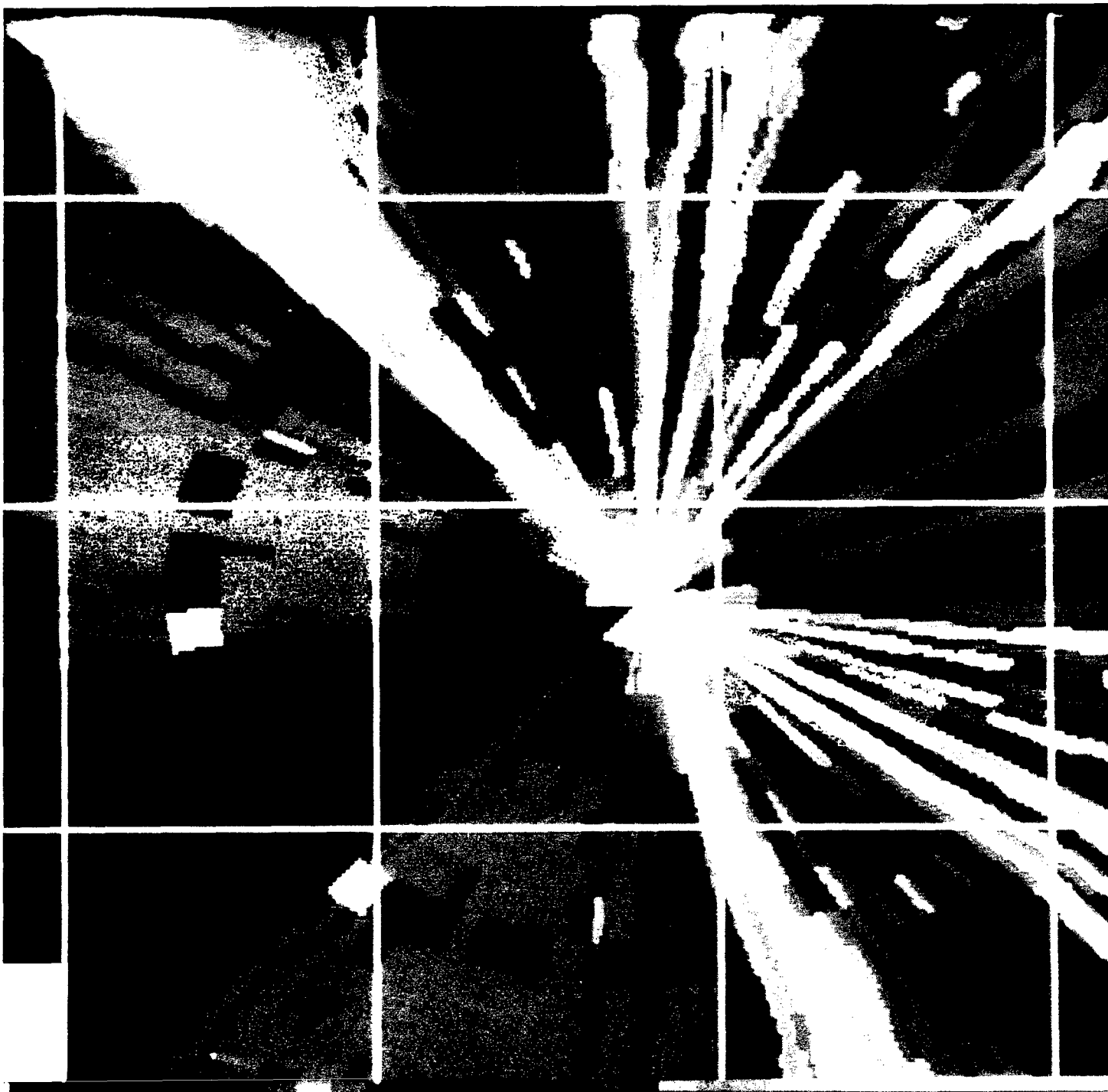0 if the point is in a shipping area or if it is a shadowed pixel

Fig. 25 — Sample map made from file MD12.DB with program NEWMAP and program APDIS (see text and Appendix B). This type of map shows regions that are contaminated by noise from distant shipping. It is used along with program ZONE to flag map regions to be omitted from further processing for this shot (No. 12).

Each output point in the SS**.DB file is written in byte format (INTEGER*1 in FORTRAN terminology), with value between -128 and 127 (inclusive). We can then transform to the latitude-longitude format with program NEWMAP (Appendix B) to produce a "single-shot scattering strength map" (MS**.DB). In Fig. 26 we show an example of such a map.

Each pixel in a MS**.DB map is $1\rlap{.}'0$ mu $1\rlap{.}'0$. The total map size is 21° 20' north-south × 21° 20' east-west (or 1280 pixels × 1280 pixels; or about 2371 km north-south × 2371 km × cos (latitude) east-west).

3.4.2 Integration of Single-Shot Maps

As we mentioned earlier, our single-shot reverberation maps contain both a *real* and a *false* image of each seamount or other topographic feature because our data were received on a linear array of hydrophones. We now discuss our method for pixel-by-pixel averaging of maps from different shots in order to eliminate the *false* topographic images and produce a clear and unambiguous topographic map.

Accumulating File

Pixels from single-shot scattering strength maps (MS**.DB) may be of three types, signal, in which case scattering strength is given; noise, in which case SS_{min} is given (SS_{min} is an upper bound on scattering strength at that pixel); or meaningless, in which case no information is given (shadowed or masked by shipping). When single-shot maps are combined into a composite map, the following four quantities are accumulated for each pixel

SIG = Average of scattering strengths appearing in this pixel,

NSIG = # of shots with signal in this pixel,

NOISE = Minimum of all SS_{mins} appearing in this pixel, and

NNOISE = Number of shots with noise in this pixel.

When a shot is added to the accumulating file (CUMU.DB), the following is done at each pixel (by program COMB.FOR), if the new shot has signal at this pixel, then NSIG is incremented by one, and the new SS value is averaged into SIG. If the new shot has this pixel labeled as noise, then NOISE is incremented and NOISE becomes min (NOISE, SS_{min}). If the new pixel is meaningful, nothing is done.

Creation of a Cumulative Scattering Strength Map

From the four accumulated variables listed above we wish to determine a single overall scattering strength estimate for each pixel. Scattering strength values are assigned according to the following chart:

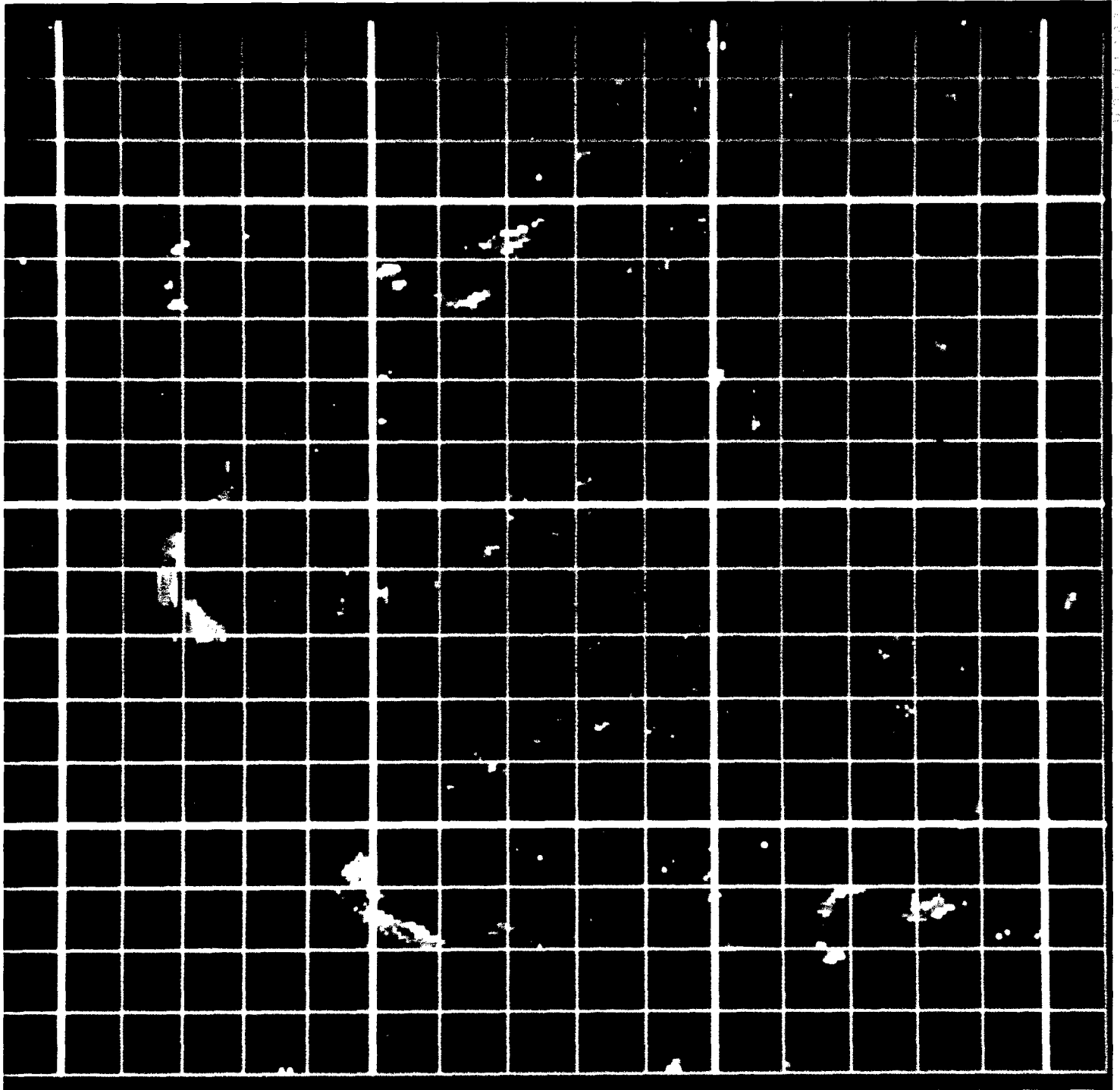|	NSIG = 0	NSIG > 0
NNOISE = 0	0	SIG
NNOISE > 0	NOISE	SIG < NOISE: SIG
		SIG > NOISE: (SIG * NSIG + NOISE * NNOISE)/ (NSIG + NNOISE)

Fig. 26 — Example of single-shot scattering strength map (shot No. 12). Scattering strength is color coded; lighter colors indicate higher scattering strength. Each topographic backscatter feature appears twice on this map because of the left-right ambiguity of the linear receiver array (see text).

All of these assignments except the last are easy to understand; if there are no signals, then NOISE is our best estimate of scattering strength. If there are signals but there are no noise pixels, then SIG is clearly the best estimate. When both signal and noise pixels are present, if SIG < NOISE, the detected signal value is less than the upper limit set by NOISE, as one would expect, hence SIG is taken as the scattering strength at that point. As usual, a zero denotes no information.

The only confusing case is SIG > NOISE; here we have an apparent contradiction, since SIG violates the upper limit set to SS by NOISE. Such a situation arises even with an ideal system, since the left-right ambiguity of the array can cause a single-shot map to contain signal in a genuinely featureless geographic location. In order for the map combination process to remove these fales images, the NOISE value must somehow contribute to the scattering strength assigned to the composite at such a point. We would not, however, want to simply take the NOISE value, because effects such as undetected shadowing can distort the NOISE figure. The weighted average of SIG and NOISE is taken instead, allowing results from different shots to average out to a reasonable value. Thus, fairly complete use is made of all legitimate data (shipping noise being illegitimate) present in the shots.

In the combined scattering strength map file (MCUM.DB), all pixels for which NSIG is less than a selected threshold (e.g., 0.3 × (# of shots)) have their scattering strength values negated (made positive) as a flag, to indicate that very few returns were received from that point. In this way, points with doubtful SS estimates can be removed from a display of the maps. This includes distant points for which SS_{min} (and hence NOISE) is rather high, and points with very few maps contributing. It also helps to cut down on the amount of residual shipping noise in the maps (see the next section).

Spatial Filtering of the Cumulative Scattering Strength Map

Examination of single-shot scattering maps shows that those areas considered as having signal present can be either topographic feature returns ("real" or "false," as described above), or residual shipping noise which has been mistaken for good data. Although strong shipping noise is supposed to be removed early on, quieter shipping and sidelobes of strong shipping still appear on the maps, especially at long ranges where large propagation loss will result in large scattering strengths when ship noise is mistaken for returns.

We do not, however, want to exclude from processing those areas with weak shipping noise, because true features can be detected in the midst of this weak noise, and one would therefore be discarding large amounts of good data by deleting these sections. A means of distinguishing this residual ship noise from the true returns *after* conversion to scattering strength would therefore be preferable.

The spatial filter provides such a method, based on the fact that true returns span several pixels and recur in the same location from shot to shot, whereas residual shipping noise is diffuse, and is distributed somewhat randomly on the map from shot to shot. Hence features will be distinguished by clusters of pixels that tend to contain signal in most shots, and residual shipping noise will cause a given pixel to be mistaken as signal in at most a few shots; those pixels that are misidentified in a substantial number of shots will be isolated, not grouped. What the filter actually does is to examine each M × N subfield of a map of NSIG values. If the total NSIG of all MN pixels in the subfield exceeds a selected threshold, then the filter takes on a value of 1 in that subfield. A pixel has filter value of 0 if it does not appear in any such subfield. The effect of the filter is to select only regions in which several pixels all contain signal in substantial number of shots. Individual isolated pixels having NSIG = 3 to 5, (i.e., some small integer value, about 1/3 the number of maps being averaged) characteristic of residual shipping noise, are removed by the filter (with proper choice of M, N, and the threshold).

The filter values are then multiplied into the MCUM data before display. Figures 27 through 29 show combined maps displayed first without, and then with, the individual pixel threshold described in the previous section, then finally the map with the spatial filter applied. The spatial filter almost completely eliminates unwanted noise, while retaining features as small as 4 × 4 pixels.

4.0 SUMMARY

This is the third report in a series on the Bathymetric Hazard Survey Test (BHST). The first two reports [Franchi and Schifter, 1980; Schifter and Franchi, 1981] discussed the sea test itself and very preliminary reverberation mapping results, and this report discusses our more extensive processing and analysis efforts during FY-1982 and FY-1984 (the project was not funded during FY-1983). These analysis efforts were aimed at:

- Improved, software-based beamforming with missing-hydrophone interpolation for improved sidelobe levels.

- Development of a remote sensing technique for estimation of seamount heights and locations in an entire ocean basin (the Canary Basin).

- Display of our reverberation-based ocean basin mapping results as a two-dimensional bathymetry map.

- Estimation of the uncertainties in our technique.

We believe that we have fulfilled these goals with the following results:

- Improved sidelobe suppression over shipboard hardware beamformer output by 5 to 7 dB.

- Analysis methodology developed to extract seamount heights from reverberation data to about ±1.3 km over an entire ocean basin.

- Location of all major basin bathymetry features to certainty of about 20 km.

- Creation of multiple-shot integrated reverberation-based ocean basin bathymetry map.

- Understanding of major sources of uncertainty in our measurement and analysis technique.

4.1 Suggestions for Further Research

We have identified possible sources of uncertainty in our technique for estimation of seamount heights and wide-area reverberation mapping (see Section 3). Based on our estimates of these sources of uncertainties, it is probable that the uncertainties in height and position could be improved by at least a factor of 2 (to ±0.7 km and ±3 km (radial) or ± 10 km (azimuthal) or smaller) by improvements in measurement and analysis techniques. The uncertainty in the ship's position could be eliminated by improved navigation (e.g., using Global Positioning System (GPS)). Improved bearing estimates could be obtained by using fixed acoustic beacons. Improved range estimates could be attained by using more accurate sound speed profile information (perhaps by dropping AXBT probes).

At present we do not know if our measured correlations of "backscattering strength measure" with seamount heights and slopes are universal or if they are unique to the Canary Basin area (see Section 2.1). Our linear regression analysis indicates that backscattering strength is linearly correlated with seamount heights with correlation coefficient approximately 0.8 and slope approxmately 7

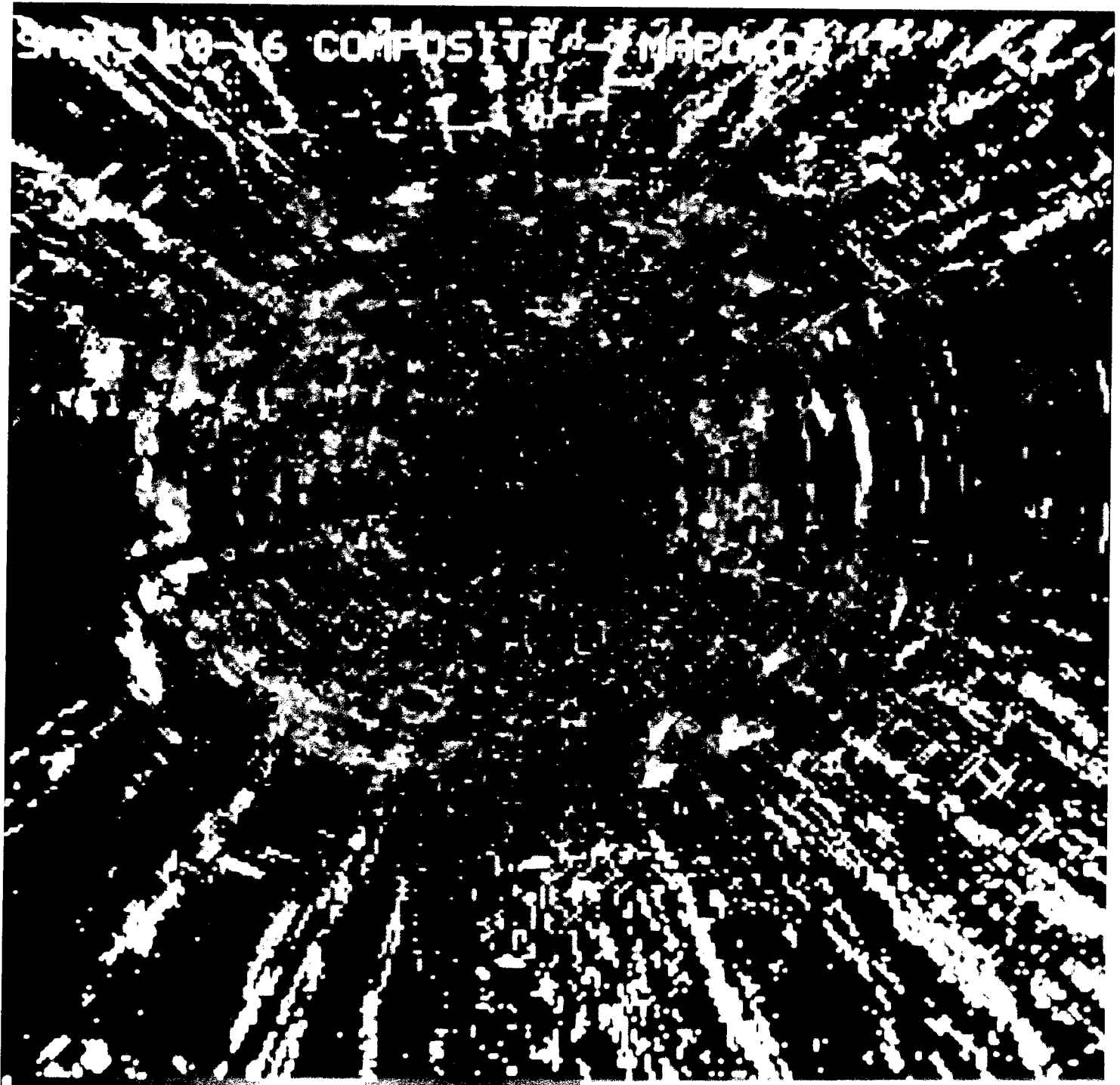Fig. 27 — Example of integrated (averaged over shots 10 through 16) scattering strength map. Contains residual shipping noise contamination at large range from shot location.

Fig. 28 — Similar to Fig. 27, but with a threshold criterion applied allowing only pixels
with three or more maps contributing to be displayed.

Fig. 29 — Similar to Fig. 28, but with a 4 × 4 pixel spatial filter applied (see text).

dB/km. Also, backscattering strength is linearly correlated with seamount slope with correlation coefficient approximately 0.5 and slope approximately 5 dB/deg. We suggest additional measurements in other ocean basins would be helpful to clarify this issue. It is likely that because of advances in computer technology, much of the processing and analysis of reverberation data in a future experiment could be accomplished on-line during the test rather than in posttest processing, thus providing quicker turn-around to final results. The ultimate image of the seafloor is likely to be a superposition of images made with different systems [Vogt and Tucholke, 1986]. The technique that we have described in this report can provide valuable quick-look mapping results for entire ocean basin areas.

5.0 ACKNOWLEDGMENTS

6.0 REFERENCES

J.A. Ballard, "Geology of a Stable Intraplate Region: The Cape Verde/Canary Basin," NORDA Report 45, NSTL Station, MS, 1982.

J.M. Brozena, "A Preliminary Analysis of the NRL Airborne Gravimetry System," *Geophysics* **49** (7) 1060-1069, (1984a).

J.M. Brozena, personal communication (1984b).

M. Czarnecki, personal communication (1984).

T.H. Dixon, M. Naraghi, M.K. McNutt, and S.M. Smith, "Bathymetric Prediction from SEASAT Altimeter Data," *J. Geophys. Res.* **88**(C3), 1563-1571 (1983).

I. Dyer, A.B. Baggeroer, J.D. Zittel, and R.J. Williams, "Acoustic Backscattering from the Basin and Margins of the Arctic Ocean," *J. Geophys. Res.* **87** (C12), 9477-9488 (1982).

I. Dyer, S.L. Jiang, and R.J. Williams, "Delineation of Eastern Arctic Ocean Features via Acoustic Backscattering," *EOS Trans.* **64** (52), 1040 (1983).

I. Dyer, "Reply," *J. Geophys. Res.* **89** (C2), 2109 (1984).

F.T. Erskine, G. Bernstein and E.R. Franchi, "Imaging Techniques for Analysis of Long Range Backscatter Data from Ocean Basin Regions," IEEE Proceedings of the Third Working Symposium on Oceanographic Data Systems, Woods Hole, MA, 160-164, 1983.

F.T. Erskine and E.R. Franchi, "Rapid, Basin-Wide Surveying of Large Undersea Topography Using Scattered Acoustic Energy," IEEE OCEANS 84 Proceedings, Washington, DC, **2**, 990-995, 1984.

F.T. Erskine, G.M. Bernstein, E.R. Franchi, and B.B. Adams, "Imaging of Long Range Reverberation from Ocean Basin Topography," *Marine Geodesy* 10 (1), 69-78 (1986).

R.H. Feden, P.R. Vogt, and H.S. Fleming, "Magnetic and Bathymetric Evidence for the 'Yermak Hot Spot' Northwest of Svalbard in the Arctic Basin," *Earth Planet. Sci. Lett.* 44, 18-38 (1979).

E.R. Franch, and D.E. Schifter, "Bathymetric Hazard Survey Test: Test Results," BHST Report No. 1, Acoustics Division, Naval Research Laboratory, Washington, DC, 1980.

E.R. Franchi, J.M. Griffin, and B.J. King, "NRL Reverberation Model: A Computer Program for the Prediction and Analysis of Medium to Long Range Boundary Reverberation," NRL Report 8721, 1984.

A. Grantz and P.E. Hart, "Are There Large Bathymetric Highs Near 73°N, 139°W in the Arctic Basin?," Comment on "Acoustic Backscattering from the Basin and Margins of the Arctic Ocean," by I. Dyer et al., *J. Geophys. Res.* 89 (C2), 2105 (1984).

R. Halley, "Acoustic Seamount Ranging with Explosive Charges," Technical Memorandum TM-234, US Navy Electronics Laboratory, San Diego, CA, 1957.

W.F. Haxby, G.D. Karner, J.L. LaBrecque and J.K. Weissel, "Digital Images of Combined Oceanic and Continental Data Sets and Their Use in Tectonic Studies," *EOS Trans. AGU* 64 (52), 995-1004 (1983).

D. Hussong, E. Silver, D. Karig, and J.G. Blackinton, "Sea MARC II Mapping of Convergent Plate Margin Features in Eastern Indonesian Waters," *EOS Trans. AGU* 64 (18), 239 (1983).

B. Luskin, M. Landisman, G.R. Tirey and G.R. Hamilton, "Submarine Topographic Echoes from Explosive Sound," *Bull. Geolog. Soc. Am.* 63, 1053-1068 (1952).

J.G. Marsh, T.V. Martin, J.J. McCarthy and P.S. Chovitz, "Mean Sea Surface Computation Using GEOS-3 Altimeter Data," *Marine Geodesy* 3, 359-378 (1980).

D.G. Schifter, E.R. Franchi, J.M. Griffin, and B.B. Adams, "Hydrographic Reconnaissance of Large Undersea Topography Using Scattered Acoustic Energy," *J. Acoust. Soc. Am.* Supplement 1, 66, S25 (1979).

D.E. Schifter and E.R. Franchi, "Bathymetric Hazard Survey Test: FY 81 Processing," BHST Report No. 2, Acoustics Division, Naval Research Laboratory, Washington, DC, 1981.

D.E. Schifter, E.R. Franchi, J.M. Griffin, and B.B. Adams, "Reverberation Mapping for Basin-Wide Bathymetric Surveys," *Marine Geodesy* 10 (1), 1-33 (1986).

R.C. Spindel and J.R. Heirtzler, "Long-Range Echo Ranging," *J. Geophys. Res.* 77 (35), 7073-7088 (1972).

R.J. VanWyckhouse, "Synthetic Bathymetric Profiling System (SYNBAPS)," Technical Report TR 233, U.S. Naval Oceanographic Office, Washington, DC, 1973.

P.R. Vogt, B. Zondek, P.W. Fell, N.Z. Cherkis, and R.K. Perry, "SEASAT Altimetry, the North Atlantic Geoid, and Evaluation by Shipborne Subsatellite Profiles," *J. Geophys. Res.* **89** (B12), 9885-9903 (1984).

P.R. Vogt and B.E. Tucholke, "Imaging the Ocean Floor: History and State of the Art," *The Geology of North America, Vol. M, The Western North Atlantic Region*, B.E. Tucholke and P.R. Vogt, eds. (Geological Society of America, 1986).

R.B. Whitmarsh, "Interpretation of Long Range Sonar Records Obtained Near the Azores," *Deep-Sea Res.*, **18**, 433-440 (1971).

R.J. Williams, "Backscattering of Low Frequency Sound from the Topographic Features of the Arctic Basin," Thesis, Massachusetts Institute of Technology, Cambridge, MA, 1981.

J.D. Zittel, Ocean Basin Reverberation. Thesis, Massachusetts Institute of Technology and Woods Hole Oceanographic Institution, Cambridge, MA, 1979.

Appendix A

STATISTICAL CONFIDENCE LIMITS FOR SEAMOUNT HEIGHT REGRESSION ANALYSIS

In our study to develop a technique for predicting topographic heights from long-range reverberation data, we performed a linear regression analysis on two variables. This results in a linear fit to the data with a linear correlation coefficient, r (e.g., Fig. 2). We wish to state confidence levels for our predicted seamount heights (Fig. 2). The following is a discussion of the relevant statistical descriptors (cf., Snedecor and Cochran [1967], and Spiegel [1961]).

We assume that our variables are Gaussian random distributed and that the independent variable is well known (this is not quite true since there is uncertainty in the SYNBAPS bathymetry, but consider it a true approximation). We are concerned with two types of confidence levels: the confidence level of the predicted mean value of Y given X, u, and a confidence level of the predicted single value of Y given X. It would be expected that one would get a tighter confidence for the mean value of Y since this would have random errors averaged out. This is in fact the case.

Consider the confidence level on a predicted mean value of Y, u, where

$$u = \hat{Y} \pm tS_y. \tag{A1}$$

Now u is the predicted mean value of Y given a particular X, and t is the deviation of the estimated mean derived from the Student's t-distribution. The confidence curves are branches of a hyperbola where the vertices are the points on the hyperbola closest to the predicted mean or single value of Y for the mean value of X, $\bar{X}$ and the minor axis is the regressive linear curve, $\hat{Y}$, for the data. This indicates that the predicted mean value of Y, u, becomes increasingly undefined as we move away from the mean value of X.

This occurs because

$$u = z + vx, \qquad \text{where } x = X - \bar{X}, \tag{A2}$$

and

$$\hat{Y} = \bar{Y} + bx, \tag{A3}$$

so

$$\hat{Y} - u = e + (b - v)x, \qquad \text{where } e = \bar{Y} - z, \tag{A4}$$

and

$$S_y = S_{y \cdot x} \times ((1/n) + (x^2/\textstyle\sum x^2))^{1/2} \tag{A5}$$

where n is the total number of points. From Eqs. (A1) and (A5) or from Eq. (A4) we see that the error grows with x.

51

Now Eq. (A1) defines the hyperbola

$$((u - \hat{Y})/b)^2 - (x/a)^2 = 1 \tag{A6}$$

$$b^2 = (tS_{y \cdot x})^2/n \tag{A7}$$

$$a^2 = (\sum x^2/n) \tag{A8}$$

$$e = (a^2 + b^2)^{1/2}/b$$

$$= ((tS_{y \cdot x})^2 + \sum x^2)^{1/2}/tS_{y \cdot x} \tag{A9}$$

so that the error will increase as x increases and $x = X - \bar{X}$, so the error increases as X moves away from $\bar{X}$.

Considering the confidence level on the predicted single value of Y given X, we have

$$Ys = \hat{Y} \pm tS_y, \tag{A10}$$

where Ys is the predicted single value of Y given a particular value of X. This also defines a hyperbola that is farther away from the regressive linear curve Y and has less curvature than the hyperbola defined by the confidence levels of the predicted mean value of Y, u. This is because there is an additional random component to the error.

$$Ys = z + vx + r, \tag{A11}$$

so

$$\hat{Y} - Ys = e + (b - v)x - r, \tag{A12}$$

and

$$S_y = S_{y \cdot x} \times ((1 + (1/n) + (x^2/\sum x^2))^{1/2}. \tag{A13}$$

Equation (A10) becomes

$$((Ys - \hat{Y})/b)^2 - (x/a)^2 = 1, \tag{A14}$$

$$a^2 = (1 + (1/n)) \sum x^2, \tag{A15}$$

$$b^2 = (tS_{x \cdot y}(1 + (1/n)))^2, \tag{A16}$$

$$e = (a^2 + b^2)/b$$

$$= ((tS_{y \cdot x})^2 + \sum x^2)^{1/2}/tS_{y \cdot x}. \tag{A17}$$

52

The eccentricities for the two hyperbolae are equal, but since the predicted single value of Y is a factor of $(n + 1)$ farther away from $\hat{Y}$ than the predicted mean value of Y, the confidence levels on the predicted single value of Y are much flatter. In other words, the asymptotes of the two curves are the same but the distance from the minor axis is a factor of $(n + 1)$ farther away.

In the case of the seamount height study, consider the predicted mean values of Y: if we had six seamounts each 3000 m high, then the average scattering strength would be −45 ±2 dB with a certain confidence level (in this case 90%). Consider, however, the single predicted value of Y: if we had a single seamount 3000 m high, then its scattering strength would be −45 ± 8 dB with a certain confidence level (90%). These errors permit us to estimate the average seamount height of approximately 3000 m to within ± 300 m. In other words, if we have 1000 returns with a scattering strength of −45 dB, then we know with a 90% confidence that the average height of these 1000 seamounts is 3000 ± 300 m. If, however, we have one reverberation measurement with a scattering strength of −45 dB, then we know the seamount is 3000 m ± 1500 m with a 90% confidence.

We are dealing with a large reverberation population (all the reverberation data), and a large seamount population (all the seamounts that cause backscatter). We have taken a selected reverberation sample and tried to extrapolate the information to the whole reverberation population. For a population that has N seamounts 3000 m high, then the average scattering strength according to our sample (Fig. 2, the inner curve) would be −45 ±2 dB with a certain confidence level (in this case 90%). If, however, we randomly pick a seamount from our population with a height of 3000 m, then its scattering strength according to our sample (Fig. 2, the outer curve) would be −45 ±8 dB with a certain confidence level (90%). These errors permit us to estimate the average seamount height of approximately 3000 m to within ± 300 m, and a single seamount height of approximately 3000 m to within ± 1500 m. To summarize, if our population has N returns with a scattering strength of −45 dB, then according to our sample we know with a 90% confidence that the average height of these N seamounts is 3000 ± 300 m. If, however, we pick one reverberation measurement from our population with a scattering strength of −45 dB, then according to our sample we know with a 90% confidence that the seamount height is 3000 ± 1500 m.

REFERENCES

G.W. Snedecor and W.G. Cochran, *Statistical Methods*, 6th ed. (Iowa State University Press, Ames, IA, 1967).

M.R. Spiegel, *Statistics* (McGraw-Hill, New York, 1961).

Appendix B

DESCRIPTION OF FORTRAN SOFTWARE FOR BHST MAP PROCESSING

REVERBERATION MAPPING FLOWCHART

```
BP**.DB

            *************
            * PreSS.FOR *                                      *************
            *************  ──────────────────►  MD**.DB  ───►  * NEWMAP.FOR *
                                                               *************
     ◄── AMBS**.DAT                                                  │
                                                                     ▼
                              *************                       MX**.DB
     ◄── LV**.DB  ◄──         * GETTL.FOR *                          │
                      ──────► *************                          ▼
                                                               *************
                                                               * APDIS.FOR *
     ◄── TL**.DAT  ◄──                                          *************
                                                                     │
                              *************                          ▼
     ◄── SHIP**.DAT ◄────────  * ZONE.FOR  * ◄──────  (COMTAL TV
                              *************             IMAGE)

**********
* SS.FOR *  ──────────────►  SS**.DB
**********                        │
                                  ▼
                          *************
                          * NEWMAP.FOR *
                          *************
                             MS**.DB
                            (OVERWRITE)
                                  │
                                  ▼
                          *************
                          *  COMB.FOR  *  ⇄  CUMU.DB
                          *************
          MCUM.DB                    MNSG.DB
                  │                  │
                  ▼   *************  ▼
                      * BLOB.FOR *
                      *************
                            │
                            ▼
                         MCUM.DB  ──────►  DISPLAY
                        (OVERWRITE)         DEVICES
```
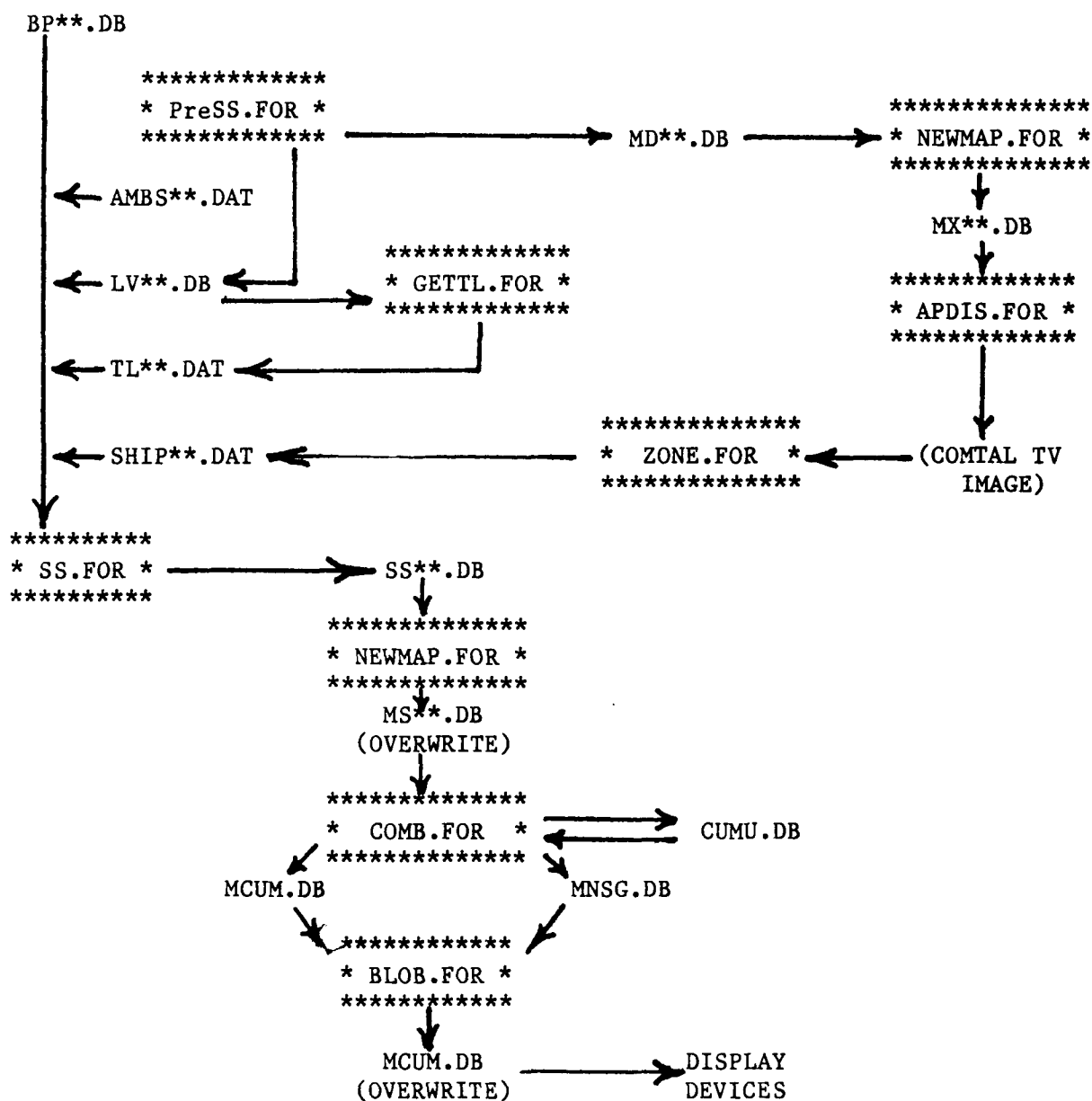
55

Table of Analysis Programs

The following table lists our reverberation mapping programs and gives the information necessary to link each. We also list input and output files for each program; files in parentheses are optional. All programs are written in FORTRAN for VAX 11/780 operating system and system library with FPS AP120B Array Processor.

Program	Subroutines	Libraries	Input Files	Output Files
NEWMAP.FOR	BLKSORT.FOR GRIDAP.VFC PACKAP.VFC SORTAP.VFC LLDBAP.VFC BNBAAP.VFC INDEX.VFC SWAP.FOR	TVLIB DBMT FPS/HSR	BP**.DB MD**.DB SS**.DB (etc.)	MP**.DB MS**.DB
PRESS.FOR	APRESS.VFC	TVLIB DBMT FPS/HSR	BP**.DB BHSTTIM.DAT	MD**.DB LV**.DB AMBS**.DAT
GETTL.FOR	MYSM.FOR	DISSPLA DBMT	LV**.DB	TL**.DAT
ZONE.FOR	—	TVLIB DBMT	MD**.DB	SHIP**.DAT
SS.FOR	APSS.VFC	DBMT FPS/HSR	BP**.DB LV**.DB AMBS**.DAT TL**.DAT SHIP**.DAT BHSTTIM.DAT	SS**.DB
COMB.FOR	APMERG.VFC APPEND.VFC	DBMT FPS/HSR	CUMU.DB (MS**.DB)	(CUMU.DB) (MCUM.DB) (MNSG.DB)
BLOB.FOR	APBLOB.VFC	DBMT FPS/HSR	MCUM.DB MNSG.DB	MCUM.DB
APDIS.FOR		TVLIB BDMT FPS/HSR	MP**.DB MS**.DB MCUM.DB MNSG.DB	
MAPDICO.FOR	 DICOGRID.FOR TRANS1.VFC TRANS2.VFC	 DBMT DISSPLA DBIMAGE FPS/HSR	MP**.DB MS**.DB MCUM.DB MNSG.DB	

DESCRIPTION OF PROGRAMS

NEWMAP.FOR—This program is designed to read files which are in a beam-time format, then to make use of array position and heading information, and to perform a geometric transformation to a latitude-longitude format.

PRESS.FOR—Does several necessary tasks before the main program SS.FOR can be run. The first section tries to find the shot in the BP**.DB file, and to identify ambient noise frames before the shot. The user observes the action on the COMTAL screen, and accepts or vetoes the program's guesses at where the shot is. Ambient noise levels for each beam are calculated and written to file AMBS**.DAT. An overall (omnidirectional) noise level is also calculated, and is written to a header in file LV**.DB along with shot time, start and stop times, and other pertinent information. The second section of this program examines the data from the start to the stop times, and finds for each frame the typical reverb level (25th percentile of beams 11-250); these are written to file LV**.DB. For each group of 200 frames, the 30th percentile of the distribution of reverb levels is found for each of the 256 beams, for use in identifying ship noise. After a correction for beamwidths, this data is written to file MD**.DB, which has a format compatible with NEWMAP.FOR to facilitate display on the COMTAL.

GETTL.FOR—Synthesizes a transmission loss curve for each shot based on a formula, and using the data from LV**.DB wherever possible as described above. Because of the difficulties described above, the resulting curve should be checked by the user before running SS.FOR visually (by running GETTL to make a plot). It is often necessary to change the default ambient noise level to get proper results. The plot produced by GETTL is also useful for determining the frame at which convergence zones end (needed by SS.FOR). Final TL estimate is placed in file TL**.DAT.

ZONE.FOR—A program that decides which sections of the map (actually of the beam-time file) will be marked as shipping noise. The program first performs simple thresholding then identifies all distinct contiguous regions that are above threshold. Regions that cover long time periods are marked as shipping noise, while shorter regions remain as good data. Note the sequence of programs on the far right of the flowchart, of which the sole purpose is to produce a TV map image which assists the user in making decisions about deletion. ZONE can send a function to the COMTAL that will white out approximately those regions that are above threshold (NOTE—the whited out regions are NOT exactly those being marked as shipping). The user can change any of the program's decisions (this is always necessary) before the results are written to file SHIP**.DAT.

SS.FOR—This is the main program, which actually computes scattering strength from reverberation data. As outlined above, reverberation data from the file BP**.DB is processed using the ambient noise, transmission loss, and shipping noise files created before, and by sometimes doing the temporal noise adjustments. The output file SS**.DB contains the SS, SS_{min}, or "no information" data. This SS**.DB file is put into map format with NEWMAP.FOR, producing the file MS**.DB.

COMB.FOR—Program that manages the accumulating map file CUMU.DB. It can be used to add another shot into the cumulative file, and/or it can produce a merged scattering strength map MCUM.DB. This program can also produce maps of any of the four statistics kept in CUMU.DB; in particular, a map file MNSG.DB of NSIG must be made to run the spatial filter.

BLOB.FOR—The spatial filter program. The two input files are MNSG.DB, a file of the NSIG data from which the filter is calculated, and MCUM.DB, the combined scattering strength map to which the filter is to be applied. The output file is the overwritten, filtered map MCUM.DB.

APDIS.FOR—This is a general purpose utility program for producing a color or grayscale display of a map file (e.g., MP**.DB) on the COMTAL. This program takes a 1024 × 1024 pixel area of a 1280 × 1280 pixel map file, and it then decimates by a factor of 4 in order to display the map on the 256 × 256 pixel screen of the COMTAL. This program also has the capability to display a small portion of the map file (about 1/4) at full resolution.

MAPDICO.FOR—This is an alternate program to APDIS.FOR for displaying map files in color or grayscale. It produce "DBMAGE" files compatible with NRL 5160 "VUGRAPH" plotting software. ("DBIMAGE" is a NRL 5160 software package that enables us to make two-dimensional color or grayscale plots on various devices.) With MAPDICO.FOR, we can display all or part of a map file on one of several devices, including the COMTAL, the CALCOMP hardcopy plotter, and the DICOMED plotter (with DISSPLA overlays if desired).